COHERENCE AND STATISTICS OF PHOTONS AND ATOMS

Edited by

Jan Peřina

2001

A Wiley-Interscience Publication
JOHN WILEY & SONS, INC.
New York • Chichester • Weinheim • Brisbane • Singapore • Toronto

7 Atoms in a Squeezed Vacuum

Ryszard Tanaś

Nonlinear Optics Division, Institute of Physics, Adam Mickiewicz University, Poznań, Poland

7.1 INTRODUCTION

Squeezed vacuum is a state of the electromagnetic field with very special properties: There are strong correlations between the field amplitudes at frequencies placed symmetrically with respect to a certain carrier frequency ω_s, and the evolution of an atom subjected to such a field exhibits a number of unique features related to quantum properties of the squeezed vacuum. Many such features are well known and described in review articles [1, 2]. In this chapter we are not going to repeat the material that can be found elsewhere, but simply present an overview of two different approaches to the interaction of an atomic system with the squeezed light of finite bandwidth. One approach deals with the squeezed vacuum of finite but sufficiently broad bandwidth, which is much broader than the atomic linewidth, and the squeezed vacuum can be treated as a Markovian reservoir to the atom. This allows for derivation of the Markovian master equation describing the evolution of the atomic system. The other approach is based on the coupled systems approach [3, 4], which allows for description of the interaction between the atom and the squeezed light with the bandwidth, which is comparable and even narrower than the atomic linewidth. Interaction of such light with the atom leads to some unexpected features in the optical spectra of the atom which will be discussed here.

Since the first paper published by Gardiner on spectroscopy with a broadband squeezed vacuum field [5], much work has been done to find new features in the resonance fluorescence and probe absorption spectra of two- and three-level atoms in a squeezed vacuum [1]. Gardiner [5] has shown that in a squeezed vacuum the atomic dipole moment can decay with two different rates, one much longer and the other much shorter than that in the normal vacuum. In consequence, a subnatural linewidth has been predicted in the spontaneous emission spectrum. The addition of a coherent driving field to

the problem introduces a strong dependence of the atom dynamics and the fluorescence spectrum on the relative phase between the coherent field and the squeezed field. Carmichael et al. [6] have shown that depending on the phase, the central peak of the Mollow triplet [7] can either be much narrower or much broader than the natural linewidth of the atom. The narrowing of the central peak relative to its normal vacuum width is possible for a squeezed vacuum with an arbitrary photon number N. However, the sidebands could be narrowed only for a sufficiently low photon number ($N < 0.125$) [8, 9] and for $N > 0.125$ are always broadened compared to their normal vacuum width. Thus, the spectrum can be modified quantitatively from the spectrum associated with the normal vacuum. Apart from the quantitative modifications, the qualitative changes in the fluorescence spectrum have also been predicted. Courty and Reynaud [10] have found that for a certain detuning of the driving field from the atomic resonance, the central peak and one of the sidebands can be suppressed due to population trapping in the dressed state. Smart and Swain [11, 12, 13] have found unusual features in the resonance fluorescence spectra, such as hole burning and dispersive profiles. These features, however, appear for Rabi frequencies comparable to the atomic linewidth and are very sensitive to the various parameters involved.

Another spectroscopic feature accessible to experimental verification is the probe absorption spectrum. Mollow [14] has predicted that the absorption spectrum of a weak field probing a system of two-level atoms driven by an off-resonant laser field consists of one absorption and one emission component at the Rabi sidebands and a small dispersion-like component at the center of the spectrum. The emission component indicates that in one sideband, stimulated emission outweighs absorption, so that the probe beam is amplified at the expense of the driving field. The probe field can be amplified due to the population inversion between the dressed states, despite the fact that there is no population inversion between the bare atomic states. Apart from the amplification at one of the Rabi sidebands, the absorption spectrum also exhibits amplification on one side of a small dispersion-like structure centered at laser frequency [15], the physical origin of which comes from the interference between absorption and emission processes and is not associated with any population inversion because the transition occurs between equally populated states on both the bare and dressed atom bases [16]. This amplification, however, vanishes when the atom is driven by a resonant laser field. Amplification without population inversion has become a subject of intensive research in recent years [17]. For a resonant driving field, however, the probe absorption spectrum exhibits dispersion-like profiles at the Rabi sidebands of a relatively small amplitude. The features have been interpreted in terms of the dressed-atom description of the field-atom interaction [18].

The asymmetry of the absorption spectrum is not only crucial in obtaining lasing without inversion but, for example, is also important in laser cooling [19]. Cirac and Zoller [20] have shown that the spectrum of fluctuations of

the dipole force, which is proportional to the absorption spectrum, can be asymmetric, even for a resonant cooling laser field, when the two quadratures of the atomic dipole decay at different rates. This is exactly the situation that occurs when a two-level atom is damped by a squeezed vacuum [21]. Apart from the asymmetry, the absorption spectrum can exhibit a strong emission peak (amplification) at the central frequency which is not attributed to population inversion in either the bare-atom or dressed-atom picture [22].

Most of the studies dealing with the problem of a two-level atom in a squeezed vacuum assume that the squeezed vacuum is broadband; i.e., the bandwidth of the squeezed vacuum is much larger than the atomic linewidth and the Rabi frequency of the driving field. Experimental realizations of squeezed states [23–26], however, indicate that the bandwidth of the squeezed light is typically on the order of the atomic linewidth. The most popular schemes for generating squeezed light are those using a parametric oscillator operating below threshold, the output of which is a squeezed beam with a bandwidth on the order of the cavity bandwidth [27, 28]. There are two types of squeezed field that can be generated by such a parametric oscillator. If the oscillator works in a degenerate regime, the squeezed field has the profile with the maximum of squeezing at the central frequency and a small squeezing far from the center. In the nondegenerate regime, the profile has two peaks at frequencies symmetrically displaced from the central frequency. For strong driving fields and finite bandwidth of squeezing, this means that the Rabi sidebands can feel quite different squeezing than the central line. A realistic description of radiative properties of the two-level atom in such a squeezed field must thus take into account the finite bandwidth of the squeezed field.

First studies of the finite-bandwidth effects have been performed by Gardiner et al. [27], Parkins and Gardiner [29], and Ritsch and Zoller [30]. The approaches were based on stochastic methods and numerical calculations and were applied to analyze the narrowing of the spontaneous emission and absorption lines. The fundamental effect of narrowing has been confirmed, but the effect of finite bandwidth was to degrade the narrowing of the spectral lines rather than enhance it. Later, however, numerical simulations done by Parkins [31, 32] demonstrated that for strong driving fields a finite bandwidth of squeezing can have positive effect on the narrowing of the Rabi sidebands. He has found that there is a difference between the two types of squeezed light generated in either the degenerate or nondegenerate regime of the parametric oscillator. In the former case it is possible to narrow either both of the Rabi sidebands or the central peak of the fluorescent spectrum, while in the latter case simultaneous narrowing of all three spectral peaks is possible.

Recently, Yeoman and Barnett [33] have proposed an analytical technique for investigating the behavior of a coherently driven atom damped by a squeezed vacuum with finite bandwidth. In their approach, they have derived a master equation and analytic expressions for the fluorescent spectrum for the simple case of a two-level atom exactly resonant with the frequencies

of both the squeezed field and the driving field. Their analytical results agree with that of Parkins [31, 32] and show explicitly that the width of the central peak of the fluorescent spectrum depends solely on the squeezing present at the Rabi sideband frequencies. They have assumed that the atom is classically driven by a resonant laser field for which the Rabi frequency is much larger than the bandwidth of the squeezed vacuum, although this is still large compared to the natural linewidth. Unlike the conventional theory, based on uncoupled states, it is possible to obtain a master equation consistent with the Born–Markov approximation by first including the interaction of the atom with the driving field exactly, and then considering the coupling of this combined dressed atom system with the finite-bandwidth squeezed vacuum. The advantage of this dressed atom method over the more complex treatments based on adjoint equation or stochastic methods [31, 32, 34] is that simple analytical expressions for the spectra can be obtained, thus displaying explicitly the factors that determine the intensities of the spectral features and their widths. Recently, the idea of Yeoman and Barnett has been extended by Ficek et al. [35] to the case of a fully quantized dressed-atom model coupled to a finite-bandwidth squeezed field inside an optical cavity. They have studied the fluorescence spectrum under the secular approximation [18] and have found that in the presence of a single-mode cavity, the effect of squeezing on the fluorescence spectrum is more evident in the linewidths of the Rabi sidebands than in the linewidth of the central component. In the presence of a two-mode cavity and a two-mode squeezed vacuum, the signature of squeezing is evident in the linewidths of all spectral lines. They have also established that the narrowing of the spectral lines is very sensitive to the detuning of the driving field from the atomic resonance. The dressed-atom method, including a detuning of the driving field from the atomic resonance, has also been applied to calculate the probe absorption spectra of a driven two-level atom in a narrow-bandwidth squeezed vacuum [36]. This method could also be applied to calculate the fluorescence spectrum.

Tanaś et al. [37] have adopted the Yeoman and Barnett [33] idea but without using the Laplace transforms and the pole approximation, and they have derived the master equation for a two-level atom driven by a classical laser field and damped by a finite-bandwidth squeezed vacuum, including a nonzero detuning of the driving field from the atomic resonance. Despite the complexity of the problem, they have obtained a quite simple master equation that is valid for arbitrary values of the Rabi frequency and the detuning but for squeezing bandwidths much greater than the natural linewidth. The corresponding optical Bloch equations for the atomic operators has been derived in a standard way from the master equation. The Bloch equations have been applied to calculate the fluorescence spectrum and the quadrature-noise (squeezing) spectrum of the scattered field. It has been found that the detuning changes considerably the shape of the resonance fluorescence spectrum and leads to novel spectral features. The squeezing spectrum allows for a simple explanation of the linewidth narrowing, hole burning, and disappearance of the

spectral lines. It turned out that for a strong resonant driving field the fluorescence field does not exhibit any squeezing, but the spectral lines can be significantly narrowed. When the atom is driven by a weak laser field, the fluorescence field exhibits a large squeezing which leads to further narrowing of the spectral lines and a hole burning. Moreover, it has been found that for some detunings the number of lines in the fluorescence spectrum does not correspond to the number of lines in the noise spectrum, in contrast to what one could expect that the fluorescence spectrum should reveal to the noise spectrum.

An alternative approach to the problem of the interaction of squeezed light with a squeezed vacuum, called the *coupled-systems* approach, has been proposed by Gardiner [3] and Carmichael [4]. This approach treats the parametric oscillator producing squeezed light as a part of the dynamical system, and the master equation is obtained that describes parallel evolution of the atom and the cavity field. Since the squeezed vacuum is not treated as the reservoir to the atom, but rather as a driving field, there is no requirement for the squeezed vacuum bandwidth to be broad. This makes it possible to study effects associated with the narrow-bandwidth squeezed vacuum. A disadvantage of this approach, however, is the fact that the master equation describing the evolution of the coupled systems does not allow for analytical solutions and one has to rely on numerical solutions only. The coupled-systems approach has been applied by Gardiner and Parkins [38], Smyth et al. [39, 40], and Messikh et al. [41] to study the effect of squeezing bandwidth on the inhibition of atomic phase decays, spectral linewidth narrowing, and the anomalous features of the optical spectra of the atom driven by a squeezed vacuum. We present some of the unusual features of such spectra in this chapter.

7.2 SOURCES OF SQUEEZED LIGHT

7.2.1 Degenerate parametric oscillator

Light with squeezed vacuum fluctuations can be obtained in many nonlinear optical processes [42], but the most effective scheme to produce squeezed light turned out to be the degenerate/nondegenerate parametric oscillator or parametric down converter (see, for example, [43] and papers cited therein). In the parametric oscillator a laser pump field at frequency $2\omega_s$ is split by a nonlinear crystal into two photons at frequencies ω_1 and ω_2 such that $\omega_1 + \omega_2 = 2\omega_s$, where ω_s is the squeezing carrier frequency. If $\omega_1 \neq \omega_2$, the parametric oscillator is said to be nondegenerate (NDPO), and when the two frequencies are equal, the parametric oscillator is referred to as degenerate (DPO). The nonlinear crystal is placed in a cavity with one mirror which is almost perfectly reflecting for the photons at ω_1 and ω_2, but transparent to the pump photons at $2\omega_s$, and the other mirror with finite transmissivity for the down-

converted photons. For the parametric oscillator working below the threshold for oscillation, the outgoing light is in a squeezed vacuum state which exhibits unique quantum properties. The properties of such light have been calculated by Collett and Gardiner [44] for DPO and extended by Collett, Loudon, and Gardiner [28] for NDPO. The output field from DPO is characterized by the following correlation functions:

$$\langle a_{out}^{+}(\omega)a_{out}(\omega')\rangle = N(\omega)\delta(\omega-\omega')\,, \tag{7.1}$$

$$\langle a_{out}(\omega)a_{out}(\omega')\rangle = M(\omega)\delta(2\omega_s-\omega-\omega')\,. \tag{7.2}$$

For a degenerate parametric oscillator, the squeezing properties are described by [44]

$$N(\omega) = \frac{\lambda^2-\mu^2}{4}\left[\frac{1}{(\omega-\omega_s)^2+\mu^2}-\frac{1}{(\omega-\omega_s)^2+\lambda^2}\right], \tag{7.3}$$

$$M(\omega) = \mathrm{e}^{i\phi}\,\frac{\lambda^2-\mu^2}{4}\left[\frac{1}{(\omega-\omega_s)^2+\mu^2}+\frac{1}{(\omega-\omega_s)^2+\lambda^2}\right]; \tag{7.4}$$

λ and μ are related to the cavity damping rate κ, and the amplitude of the pump field ϵ of the parametric oscillator according to

$$\lambda = \frac{\kappa}{2}+\epsilon\,, \qquad \mu = \frac{\kappa}{2}-\epsilon\,, \tag{7.5}$$

and ϕ is the phase of the pump field.

From (7.1) it is clear that $N(\omega)$ is related to the mean number of photons at frequency ω, while $M(\omega)$ is characteristic of the squeezed vacuum field and describes the correlation between the two photons created in the down-conversion process. The frequency dependence of the two parameters $N(\omega)$ and $M(\omega)$ is governed by two Lorentzian functions with widths λ and μ defined by the cavity damping rate and the amplitude of the pump field. Below threshold, $\epsilon < \kappa/2$, both λ and μ are positive, and $\lambda > \mu$. In the case of the parametric oscillator, we have

$$|M(\omega)| = \sqrt{N(\omega)[N(\omega)+1]}\,, \tag{7.6}$$

which means that the output field is an *ideal squeezed vacuum.* Generally, however, $|M(\omega)| \le \sqrt{N(\omega)[N(\omega)+1]}$, and only when $|M(\omega)| > N(\omega)$ is the field strictly quantum, without classical analogue. For $|M(\omega)| \le N(\omega)$ the field can be considered as a classically squeezed field. The most interesting phenomena are those which appear only in the region of quantum squeezing, where $N(\omega) < |M(\omega)| \le \sqrt{N(\omega)[N(\omega)+1]}$.

In many cases the frequency dependence of $N(\omega)$ and $M(\omega)$ can be omitted and the squeezed vacuum becomes the *broadband squeezed vacuum.* This happens when λ and μ are much larger than all other relaxation rates in

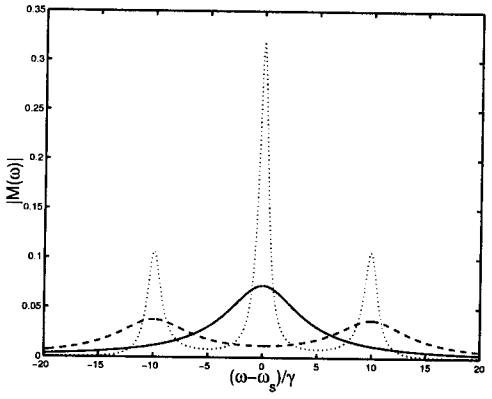

Fig. 7.1 Plots of $|M(\omega)|$ for DPO (solid line) and NDPO (dashed line) for $\alpha = 10$. The parameters are: $\kappa/\gamma = 10$ and $\epsilon/\kappa = 0.125$. For reference we plot the Mollow triplet for the Rabi frequency $\Omega = \alpha = 10$ (dotted line). All frequencies are scaled in units of the atomic linewidth γ.

the problem. In such situations the squeezed vacuum is parametrized by two constants N and M.

7.2.2 Nondegenerate parametric oscillator

When the parametric oscillator works in the nondegenerate regime (NDPO) the frequency dependence of $N(\omega)$ and $M(\omega)$ is given by [28]

$$N(\omega) = \frac{\lambda^2-\mu^2}{8}\left[\frac{1}{(\omega-\omega_s-\alpha)^2+\mu^2}+\frac{1}{(\omega-\omega_s+\alpha)^2+\mu^2}\right.$$
$$\left.-\frac{1}{(\omega-\omega_s-\alpha)^2+\lambda^2}-\frac{1}{(\omega-\omega_s+\alpha)^2+\lambda^2}\right], \tag{7.7}$$

$$M(\omega) = \mathrm{e}^{i\phi}\frac{\lambda^2-\mu^2}{8}\left[\frac{1}{(\omega-\omega_s-\alpha)^2+\mu^2}+\frac{1}{(\omega-\omega_s+\alpha)^2+\mu^2}\right.$$
$$\left.+\frac{1}{(\omega-\omega_s-\alpha)^2+\lambda^2}+\frac{1}{(\omega-\omega_s+\alpha)^2+\lambda^2}\right]. \tag{7.8}$$

The parameter $\alpha = (\omega_1-\omega_2)/2$ is characteristic of a two-mode squeezed field generated by the nondegenerate parametric oscillator and represents the displacement from the central frequency of the squeezing at which the two-mode squeezed vacuum is maximally squeezed.

Similarly to the DPO, the squeezed vacuum generated by NDPO satisfies the relation $|M(\omega)| = \sqrt{N(\omega)[N(\omega)+1]}$; i.e., the field is the ideal squeezed vacuum. If the broadband approximation is made, there is no difference be-

tween the field from DPO and NDPO; both can be described by the parameters N and M, which are constants (Fig. 7.1). However, if λ and μ are finite, the two fields differ dramatically: DPO produces a field with one peak centered at the squeezing carrier frequency, while NDPO produces light with two spectral peaks symmetrically shifted by α with respect to the carrier frequency ω_s. This fact can have important consequences when, for example, an atom interacts with the squeezed vacuum. If μ is much greater than the atomic linewidth γ, the broadband approximation can be used, and the squeezed vacuum can be treated as a reservoir to the atom. In Fig. 7.1 we have plotted examples of the squeezing parameters $|M(\omega)|$ as a function of ω for DPO and NDPO assuming that $\kappa/\gamma = 10$ and $\epsilon/\kappa = 0.125$. The frequency is scaled in units of the atomic linewidth γ. For NDPO we assume that $\alpha/\gamma = 10$, which means that NDPO produces two lines shifted with respect to the squeezing carrier frequency ω_s by α. To visualize better the effect that a squeezed vacuum of given type can have on the atom driven by a strong classical field, we have added for reference the standard fluorescence spectrum, i.e., the Mollow triplet with the Rabi frequency $\Omega = \alpha$. Clearly, the central line and the sidebands can feel quite different squeezing, depending on the regime in which the parametric oscillator is operating. Some consequences of this fact are discussed later in this chapter.

7.3 SQUEEZED VACUUM AS A RESERVOIR: MARKOVIAN MASTER EQUATION

Let us consider a two-level atom driven by a detuned monochromatic laser field and damped by a squeezed vacuum with finite bandwidth. Adopting the idea of Yeoman and Barnett [33], which is based on the model proposed earlier by Carmichael and Walls [45] and Cresser [46], Tanaś et al. [37] have derived a master equation for the system, which includes squeezing bandwidth effects. In this approach, the dressing transformation is performed first, to include the interaction of the atom with the driving field, and next, the resulting dressed atom is coupled to the narrow-bandwidth squeezed vacuum field. We introduce here this approach in a systematic way.

We derive the master equation under the Markov approximation which requires the squeezing bandwidth to be much greater than the atomic linewidth, but not necessarily greater than the Rabi frequency of the driving field and the detuning. For simplicity, we assume that the squeezing properties are symmetric about the central frequency of the squeezed field, which, in turn, is exactly equal to the laser frequency. Our model differs from that of Yeoman and Barnett in adding a nonzero detuning which, as has been shown in [37], leads to new and interesting effects. Contrary to Yeoman and Barnett [33], who used the Laplace transform method and the pole approximation, we perform all calculations in the time domain. There are some discrepancies be-

tween the two approaches which have been discussed in [37]. Here, we present and apply our version of the master equation.

We start from the Hamiltonian of the system which, in the rotating-wave and electric-dipole approximations, is given by

$$H = H_A + H_R + H_L + H_I\,, \tag{7.9}$$

where

$$H_A = \frac{1}{2}\hbar\omega_A\,\sigma_z = -\frac{1}{2}\hbar\Delta\,\sigma_z + \frac{1}{2}\hbar\,\omega_L\,\sigma_z \tag{7.10}$$

is the Hamiltonian of the atom,

$$H_R = \hbar\int_0^\infty \omega\, b^+(\omega)\, b(\omega)\,\mathrm{d}\omega \tag{7.11}$$

is the Hamiltonian of the vacuum field,

$$H_L = \frac{1}{2}\hbar\Omega\left[\sigma_+\exp(-i\omega_L t) + \sigma_-\exp(i\omega_L t)\right] \tag{7.12}$$

is the interaction Hamiltonian between the atom and the classical laser field, and

$$H_I = i\hbar\int_0^\infty K(\omega)\left[\sigma_+\, b(\omega) - b^+(\omega)\,\sigma_-\right]\mathrm{d}\omega \tag{7.13}$$

is the interaction Hamiltonian of the atom with the vacuum field. In (7.10)–(7.13), $K(\omega)$ is the coupling of the atom to the vacuum modes, $\Delta = \omega_L - \omega_A$ is the detuning of the driving laser field frequency ω_L from the atomic resonance ω_A, and σ_+, σ_-, and σ_z are the Pauli pseudo-spin operators describing the two-level atom. The laser driving field strength is given by the Rabi frequency Ω, while the operators $b(\omega)$ and $b^+(\omega)$ are the annihilation and creation operators for the vacuum modes satisfying the commutation relation

$$[b(\omega), b^+(\omega')] = \delta(\omega - \omega')\,. \tag{7.14}$$

For simplicity, we assume that the laser field phase is equal to zero ($\phi_L = 0$).

In order to derive the master equation we perform the two-step unitary transformation. In the first step we use the second part of the atomic Hamiltonian (7.10) and the free field Hamiltonian (7.11) to transform to the frame rotating with the laser frequency ω_L and to the interaction picture with respect to the vacuum modes. After this transformation our system is described by the Hamiltonian

$$H_0 + H_I^{(r)}(t)\,, \tag{7.15}$$

where

$$H_0 = -\frac{1}{2}\hbar\Delta\sigma_z + \frac{1}{2}\hbar\Omega(\sigma_+ + \sigma_-) \tag{7.16}$$

and

$$\begin{aligned} H_I^{(r)}(t) &= i\hbar\int_0^\infty K(\omega)\Big\{\sigma_+\, b(\omega)\, \exp[i(\omega_L-\omega)\,t] \\ &\quad - b^+(\omega)\,\sigma_-\, \exp[-i(\omega_L-\omega)\,t]\Big\}\,\mathrm{d}\omega\,. \end{aligned} \tag{7.17}$$

The second step is the unitary dressing transformation performed with the Hamiltonian H_0, given by (7.16). The transformation

$$\sigma_\pm(t) = \exp\left(-\frac{i}{\hbar}H_0 t\right)\sigma_\pm \exp\left(\frac{i}{\hbar}H_0 t\right) \tag{7.18}$$

leads to the following time-dependent atomic raising and lowering operators

$$\sigma_\pm(t) = \frac{1}{2}\left[\mp(1\pm\tilde{\Delta})\tilde{\sigma}_- \exp(-i\Omega' t) \pm (1\mp\tilde{\Delta})\tilde{\sigma}_+ \exp(i\Omega' t) + \tilde{\Omega}\tilde{\sigma}_z\right], \tag{7.19}$$

where

$$\begin{aligned} \tilde{\sigma}_- &= \frac{1}{2}\left[(1-\tilde{\Delta})\sigma_- - (1+\tilde{\Delta})\sigma_- - \tilde{\Omega}\sigma_z\right], \\ \tilde{\sigma}_+ &= \frac{1}{2}\left[-(1+\tilde{\Delta})\sigma_- + (1-\tilde{\Delta})\sigma_+ - \tilde{\Omega}\sigma_z\right], \\ \tilde{\sigma}_z &= \tilde{\Omega}(\sigma_- + \sigma_+) - \tilde{\Delta}\sigma_z \end{aligned} \tag{7.20}$$

are the "dressed" operators oscillating at frequencies $-\Omega'$, Ω', and 0, respectively, and

$$\tilde{\Omega} = \frac{\Omega}{\Omega'}, \quad \tilde{\Delta} = \frac{\Delta}{\Omega'}, \quad \Omega' = \sqrt{\Omega^2+\Delta^2}\,. \tag{7.21}$$

We assume that $\Omega' > 0$, so for weak fields, $\Omega \sim 0$, the dressed operators $\tilde{\sigma}_\pm \to \sigma_\pm$, $\tilde{\sigma}_z \to \sigma_z$ for $\Delta < 0$, and $\tilde{\sigma}_\pm \to -\sigma_\mp$, $\tilde{\sigma}_z \to -\sigma_z$ for $\Delta > 0$.

Under the transformation (7.19) the interaction Hamiltonian takes the form

$$\begin{aligned} H_I(t) &= i\hbar\int_0^\infty K(\omega)\Big\{\sigma_+(t)b(\omega)\exp[i(\omega_L-\omega)\,t] \\ &\quad - b^+(\omega)\sigma_-(t)\exp[-i(\omega_L-\omega)\,t]\Big\}\,\mathrm{d}\omega\,. \end{aligned} \tag{7.22}$$

The master equation for the reduced density operator ρ of the system can be derived using standard methods [47]. In the Born approximation the equation

of motion for the reduced density operator is given by [47]

$$\frac{\partial \rho^{(d)}}{\partial t} = -\frac{1}{\hbar^2}\int_0^t \mathrm{Tr}_R\left\{[H_I(t),[H_I(t-\tau),\rho_R(0)\rho^{(d)}(t-\tau)]]\right\}\,\mathrm{d}\tau\,, \quad (7.23)$$

where the superscript d stands for the dressed picture, $\rho_R(0)$ is the density operator for the field reservoir, Tr_R is the trace over the reservoir states, and the Hamiltonian $H_I(t)$ is given by (7.22). We next make the Markov approximation [47] by replacing $\rho^{(d)}(t-\tau)$ in (7.23) by $\rho^{(d)}(t)$, substitute the Hamiltonian (7.22), and take the trace over the reservoir variables. Since the squeezed vacuum plays the role of the reservoir to the atom, the reservoir operators $b(\omega)$ and $b^+(\omega)$ are the operators $a_{out}(\omega)$ and $a^+_{out}(\omega)$ from equation (7.1), and we have

$$\begin{aligned}
\mathrm{Tr}_R[b(\omega)b^+(\omega')\rho_R(0)] &= \langle b(\omega)b^+(\omega')\rangle = [N(\omega)+1]\,\delta(\omega-\omega')\,,\\
\mathrm{Tr}_R[b^+(\omega)b(\omega')\rho_R(0)] &= \langle b^+(\omega)b(\omega')\rangle = N(\omega)\,\delta(\omega-\omega')\,, \qquad (7.24)\\
\mathrm{Tr}_R[b(\omega)\,b(\omega')\rho_R(0)] &= \langle b(\omega)\,b(\omega')\rangle = M(\omega)\,\delta(2\omega_L-\omega-\omega')\,,
\end{aligned}$$

where $N(\omega)$ and $M(\omega)$ are the squeezing parameters given by (7.3) and (7.4) for the squeezed vacuum produced by DPO, and by (7.7) and (7.8) for the squeezed vacuum produced by NDPO with the carrier frequency of the squeezed field ω_s being equal to the laser frequency ω_L.

In the Markov approximation we can extend the upper limit of the integration over τ to infinity and next perform necessary integrations using the formula

$$\int_0^\infty \exp(\pm i\,\epsilon\,\tau)\,\mathrm{d}\tau = \pi\,\delta(\epsilon) \pm i\,\mathcal{P}\frac{1}{\epsilon}\,, \quad (7.25)$$

where $\mathcal{P}$ means the Cauchy principal value. After performing all the integrations and transforming back from the dressed picture to the original density operator, in the frame rotating with the laser frequency ω_L, we finally arrive at the master equation of the form [37]

$$\begin{aligned}
\dot\rho \;=\; & \frac{1}{2}\,i\,\delta\,[\sigma_z,\rho] - \frac{1}{2}\,i\,\Omega\,[\sigma_+ + \sigma_-,\rho]\\
& + \frac{1}{2}\,\gamma\,\tilde N\,(2\,\sigma_+\rho\,\sigma_- - \sigma_-\sigma_+\rho - \rho\,\sigma_-\sigma_+)\\
& + \frac{1}{2}\,\gamma\,(\tilde N+1)\,(2\,\sigma_-\rho\,\sigma_+ - \sigma_+\sigma_-\rho - \rho\,\sigma_+\sigma_-)\\
& - \gamma\,\tilde M\,\sigma_+\rho\,\sigma_+ - \gamma\,\tilde M^*\,\sigma_-\rho\,\sigma_-\\
& + \frac{1}{4}\,i\,(\,\Lambda\,[\sigma_+,[\sigma_z,\rho]] - \Lambda^*[\sigma_-,[\sigma_z,\rho]]\,)\,, \qquad (7.26)
\end{aligned}$$

where γ is the natural atomic linewidth,

$$\tilde{N} = N(\omega_L + \Omega') + \frac{1}{2}(1 - \tilde{\Delta}^2)\, D_r\,, \tag{7.27}$$

$$\tilde{M} = M(\omega_L + \Omega') - \frac{1}{2}(1 - \tilde{\Delta}^2)\, D + i\,\tilde{\Delta}\,\delta_M\,, \tag{7.28}$$

$$\delta = \Delta + \gamma\left[\tilde{\Delta}\,\delta_N - \frac{1}{2}(1 - \tilde{\Delta}^2)\, D_i\right], \tag{7.29}$$

$$\Lambda = \gamma\tilde{\Omega}\left[\delta_N + \delta_M - i\,\tilde{\Delta}\, D\right], \tag{7.30}$$

$$D = N(\omega_L) - N(\omega_L + \Omega') - [M(\omega_L) - M(\omega_L + \Omega')]\,, \tag{7.31}$$

$$\delta_N = \frac{1}{\pi}\mathcal{P}\int_{-\infty}^{\infty} \frac{N(x)}{x + \Omega'}\,\mathrm{d}x\,, \tag{7.32}$$

$$\delta_M = \frac{1}{\pi}\mathcal{P}\int_{-\infty}^{\infty} \frac{M(x)}{x + \Omega'}\,\mathrm{d}x\,, \tag{7.33}$$

where $x = \omega - \omega_s = \omega - \omega_L$, and we have to remember that $M(\omega)$ is a complex quantity $[M(\omega) = |M(\omega)|\exp(i\phi)]$ with ϕ being the phase of squeezing. To simplify notation, we use the convention that for any complex number Q,

$$Q = Q_r + i\,Q_i \tag{7.34}$$

with the real part Q_r and the imaginary part Q_i.

In the derivation of equation (7.26) we have assumed that the phase ϕ does not depend on frequency [48], and we have included the divergent frequency shifts (the Lamb shift) to the redefinition of the atomic transition frequency [47]. Moreover, we have assumed that the squeezed vacuum is symmetric about the central frequency ω_L, so that $N(\omega_L - \Omega') = N(\omega_L + \Omega')$, and a similar relation holds for $M(\omega)$.

The master equation (7.26) has the standard form known from the broadband squeezing approaches with the new effective squeezing parameters $\tilde{N}$ and $\tilde{M}$ given by (7.27) and (7.28). There are also new terms, proportional to Λ, which are essentially narrow-bandwidth modifications to the master equation. All the narrow-bandwidth modifications are determined by the parameter D, defined in (7.31) and describing the difference between the squeezing at the center and that at the sideband, and the shifts δ_N and δ_M defined in (7.32) and (7.33). These parameters become zero when the squeezing bandwidth goes to infinity and the master equation (7.26) goes over into the corresponding master equation for the broadband squeezed vacuum [6].

The squeezing-induced shifts δ_N and δ_M depend on the explicit form of $N(\omega)$ and $M(\omega)$. Since there are two types of squeezed field that can be

generated by the parametric oscillator, $N(\omega)$ and $M(\omega)$ are given by (7.3) and (7.4) for DPO, or by (7.7) and (7.8) for NDPO.

The Cauchy principal values of the integrals (7.33) and (7.32) can be evaluated using the contour integration, which gives [33]

$$\begin{aligned} \delta_N &= \delta_\mu - \delta_\lambda \,, \\ \delta_M &= \mathrm{e}^{i\phi}(\delta_\mu + \delta_\lambda) \,, \end{aligned} \tag{7.35}$$

where the form of δ_μ and δ_λ depends on the type of squeezing being considered and is explicitly given by:

(i) for DPO

$$\delta_\mu = \Omega' \frac{\lambda^2 - \mu^2}{4} \frac{1}{\mu\,(\Omega'^2 + \mu^2)} \,, \tag{7.36}$$

$$\delta_\lambda = \Omega' \frac{\lambda^2 - \mu^2}{4} \frac{1}{\lambda\,(\Omega'^2 + \lambda^2)} \,, \tag{7.37}$$

and (ii) for NDPO with $\alpha = \Omega'$

$$\delta_\mu = \Omega' \frac{\lambda^2 - \mu^2}{4} \frac{1}{\mu\,(4\,\Omega'^2 + \mu^2)} \,, \tag{7.38}$$

$$\delta_\lambda = \Omega' \frac{\lambda^2 - \mu^2}{4} \frac{1}{\lambda\,(4\,\Omega'^2 + \lambda^2)} \,. \tag{7.39}$$

The shifts coming from the principal value terms (7.32) and (7.33) are different for the squeezed vacuum from DPO and NDPO, but they become negligible both for very small and very large Ω' as compared to λ and μ. For moderate values of Ω', the shifts are important and have to be taken into account when calculating atomic radiative properties.

7.3.1 Bloch equations

From the master equation (7.26) we easily derive the optical Bloch equations for the mean values of the atomic operators, which can be written in matrix form as

$$\frac{\mathrm{d}}{\mathrm{d}t} \begin{pmatrix} \langle \sigma_- \rangle \\ \langle \sigma_+ \rangle \\ \langle \sigma_z \rangle \end{pmatrix} = \mathbf{A} \begin{pmatrix} \langle \sigma_- \rangle \\ \langle \sigma_+ \rangle \\ \langle \sigma_z \rangle \end{pmatrix} - \begin{pmatrix} 0 \\ 0 \\ \gamma \end{pmatrix} , \tag{7.40}$$

where the matrix $\mathbf{A}$ has the form

$$\mathbf{A} = \begin{pmatrix} -\Gamma + i\,\delta & -\gamma\,\tilde{M} & \frac{i}{2}\Omega \\ -\gamma\,\tilde{M}^* & -\Gamma - i\,\delta & -\frac{i}{2}\Omega \\ i\,(\Omega + \Lambda^*) & -i\,(\Omega + \Lambda) & -2\,\Gamma \end{pmatrix}, \tag{7.41}$$

where

$$\Gamma = \frac{\gamma}{2}(1 + 2\tilde{N})\,. \tag{7.42}$$

Defining the Hermitian operators σ_x and σ_y as

$$\sigma_x = \frac{1}{2}(\sigma_- + \sigma_+)\,, \qquad \sigma_y = \frac{1}{2i}(\sigma_- - \sigma_+)\,, \tag{7.43}$$

we get from (7.40) the following equations of motion for the atomic Bloch vector components

$$\frac{\mathrm{d}}{\mathrm{d}t}\begin{pmatrix} \langle\sigma_x\rangle \\ \langle\sigma_y\rangle \\ \langle\sigma_z\rangle \end{pmatrix} = \mathbf{B}\begin{pmatrix} \langle\sigma_x\rangle \\ \langle\sigma_y\rangle \\ \langle\sigma_z\rangle \end{pmatrix} - \begin{pmatrix} 0 \\ 0 \\ \gamma \end{pmatrix}, \tag{7.44}$$

where

$$\mathbf{B} = \begin{pmatrix} -\Gamma - \gamma\tilde{M}_r & -\delta - \gamma\tilde{M}_i & 0 \\ \delta - \gamma\tilde{M}_i & -\Gamma + \gamma\tilde{M}_r & \frac{1}{2}\,\Omega \\ 2\,\Lambda_i & -2\,(\Omega + \Lambda_r) & -2\,\Gamma \end{pmatrix}. \tag{7.45}$$

From the form of the matrix $\mathbf{B}$ it is evident that the two quadrature components of the Bloch vector $\langle\sigma_x\rangle$ and $\langle\sigma_y\rangle$ have two different decay rates

$$\begin{aligned} \gamma_x &= \Gamma + \gamma\tilde{M}_r = \gamma\left(\frac{1}{2} + \tilde{N} + \tilde{M}_r\right), \\ \gamma_y &= \Gamma - \gamma\tilde{M}_r = \gamma\left(\frac{1}{2} + \tilde{N} - \tilde{M}_r\right), \end{aligned} \tag{7.46}$$

the effect known already from the Gardiner paper [5], but now the modified parameters $\tilde{N}$, given by (7.27), and $\tilde{M}$, given by (7.28), take into account the fact that the squeezed vacuum has finite bandwidth. On resonance, $\tilde{\Delta} = 0$, the two rates take the following form:

$$\begin{aligned} \gamma_x &= \gamma\left\{\frac{1}{2} + N(\omega_L + \Omega') + M_r(\omega_L + \Omega')\right\}, \\ \gamma_y &= \gamma\left\{\frac{1}{2} + N(\omega_L) - M_r(\omega_L)\right\}, \end{aligned} \tag{7.47}$$

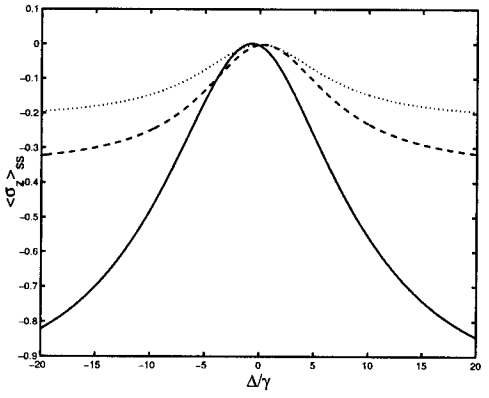

Fig. 7.2 Plots of $\langle\sigma_z\rangle_{ss}$ as a function of Δ for $\Omega/\gamma = 10$, $\phi = \pi/2$, $\epsilon/\kappa = 0.25$, $\kappa/\gamma = 20$ for DPO (solid line) and NDPO (dashed line). Dotted line marks broadband squeezing ($\kappa/\gamma = 10^5$) result.

which shows that the damping rate of $\langle\sigma_x\rangle$ is defined by the squeezing properties at the sidebands while the damping rate of $\langle\sigma_y\rangle$ is defined by the squeezing properties at the center of the spectrum. For the finite-bandwidth squeezed vacuum this fact has very important consequences. For broadband squeezing the Bloch equations (7.44) reproduce the results of Lane et al. [6].

7.3.2 Steady-state solutions

The Bloch equations (7.44) can easily be solved for the steady-state values of the atomic variables, and the result is given by

$$\begin{aligned}
\langle\sigma_x\rangle_{ss} &= \frac{1}{2}\gamma\frac{\Omega\,(\delta+\gamma\tilde{M}_i)}{d}\,,\\
\langle\sigma_y\rangle_{ss} &= -\frac{1}{2}\gamma\frac{\Omega\,(\Gamma+\gamma\tilde{M}_r)}{d}\,,\\
\langle\sigma_z\rangle_{ss} &= -\gamma\frac{\Gamma^2+\delta^2-|\gamma\tilde{M}|^2}{d}\,,
\end{aligned} \tag{7.48}$$

where

$$\begin{aligned}
d \;=\; & \Omega(\Omega+\Lambda_r)(\Gamma+\gamma\tilde{M}_r)+\Omega\Lambda_i\,(\delta+\gamma\tilde{M}_i)\\
& +2\Gamma(\Gamma^2+\delta^2-|\gamma\tilde{M}|^2)\,.
\end{aligned} \tag{7.49}$$

In Fig. 7.2 we plot $\langle\sigma_z\rangle_{ss}$ as a function of Δ for finite-bandwidth DPO and NDPO squeezing in comparison to the broadband squeezing result. The quantity $I(\Delta) = \langle\sigma_z\rangle_{ss} + 1$ expresses the steady-state fluorescence light intensity.

The expression is also known as the absorption spectrum of the driving field or stationary lineshape [49]. For both broad- and narrow-bandwidth squeezed vacuum, the absorption spectrum is a Lorentzian whose bandwidth depends on the bandwidth of the squeezed vacuum as well as on the type of squeezing that atom is subjected to, i.e., the squeezing from DPO or NDPO. Moreover, for $\phi = \pi/2$ and a narrow-bandwidth squeezed vacuum of DPO, the maximum of the Lorentzian is shifted toward negative detunings. The shift is definitely a narrow-bandwidth feature in the absorption spectrum, which cannot be observed in broadband squeezing [37].

The steady-state solutions (7.48) exhibit even more interesting features. For a resonant driving field ($\Delta = 0$), we find from (7.28) and (7.29) that

$$\delta + \tilde{M}_i = |M(\omega_A)| \sin\phi\,, \tag{7.50}$$

indicating that even for $\Delta = 0$ the $\langle\sigma_x\rangle_{ss}$ component of the Bloch vector can have a nonzero steady-state solution provided that the phase ϕ is different from 0 or π and there is a nonzero squeezing at the atomic resonance. This effect can lead to unequal populations of the dressed states of the system [50], which has interesting consequences. This point becomes more transparent when the dressed atom picture is invoked.

7.3.3 Dressed atom picture

The transformation (7.20) between the dressed atomic operators and the bare operators can be rewritten in matrix form as

$$\begin{pmatrix} \tilde{\sigma}_- \\ \tilde{\sigma}_+ \\ \tilde{\sigma}_z \end{pmatrix} = \mathbf{T} \begin{pmatrix} \sigma_- \\ \sigma_+ \\ \sigma_z \end{pmatrix}, \tag{7.51}$$

where the transformation matrix $\mathbf{T}$ has the form

$$\mathbf{T} = \begin{pmatrix} \frac{1}{2}(1-\tilde{\Delta}) & -\frac{1}{2}(1+\tilde{\Delta}) & -\frac{1}{2}\tilde{\Omega} \\ -\frac{1}{2}(1+\tilde{\Delta}) & \frac{1}{2}(1-\tilde{\Delta}) & -\frac{1}{2}\tilde{\Omega} \\ \tilde{\Omega} & \tilde{\Omega} & -\tilde{\Delta} \end{pmatrix}. \tag{7.52}$$

The inverse transformation $\mathbf{T}^{-1}$, from the dressed operators to the bare operators, can be performed with the matrix of exactly the same form as (7.52) but with $\tilde{\Omega}$ replaced by $-\tilde{\Omega}$. From the transformation (7.51), in particular by looking at the last row of the transformation matrix (7.52), it is clear that the Hamiltonian (7.16) in the dressed operators takes the diagonal form

$$H_0 = \frac{1}{2}\hbar\Omega'\tilde{\sigma}_z \tag{7.53}$$

with Ω' given by (7.21).

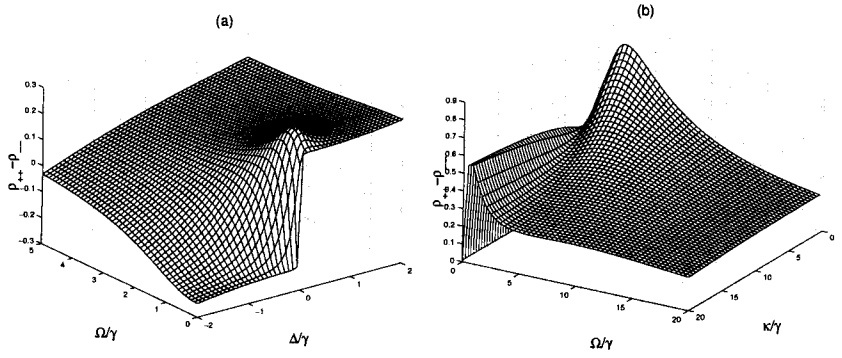

Fig. 7.3 Population inversion $\rho_{++} - \rho_{--}$ of the dressed states for the DPO squeezing with $\epsilon/\kappa = 0.25$, $\phi = \pi/2$, and (a) $\kappa/\gamma = 20$, (b) $\Delta = 0$.

An alternative way to look at the dressed atom is to introduce the dressed states (see, for example, [51]). The dressed states that diagonalize the Hamiltonian (7.16) can easily be found, and they take the following form:

$$\begin{aligned} |+\rangle &= \sqrt{\frac{1+\tilde{\Delta}}{2}}\,|g\rangle + \sqrt{\frac{1-\tilde{\Delta}}{2}}\,|e\rangle\,, \\ |-\rangle &= -\sqrt{\frac{1-\tilde{\Delta}}{2}}\,|g\rangle + \sqrt{\frac{1+\tilde{\Delta}}{2}}\,|e\rangle \end{aligned} \tag{7.54}$$

with the energies $E_\pm = \pm\hbar\Omega'/2$, and the states $|g\rangle$ and $|e\rangle$ being the ground and excited states of the atom, respectively. In terms of the dressed states the dressed operators can be expressed as

$$\tilde{\sigma}_- = |-\rangle\langle+|\,, \quad \tilde{\sigma}_+ = |+\rangle\langle-|\,, \quad \tilde{\sigma}_z = |+\rangle\langle+| - |-\rangle\langle-|. \tag{7.55}$$

The populations of the dressed states are related to the expectation values of the atomic dipole moment, or the Bloch vector, by the relations

$$\begin{aligned} \rho_{++} &= \frac{1}{2}(1 + \langle\tilde{\sigma}_z\rangle) = \frac{1}{2}\left(1 - \tilde{\Delta}\,\langle\sigma_z\rangle_{ss}\right) + \tilde{\Omega}\,\langle\sigma_x\rangle_{ss}\,, \\ \rho_{--} &= \frac{1}{2}(1 - \langle\tilde{\sigma}_z\rangle) = \frac{1}{2}\left(1 + \tilde{\Delta}\,\langle\sigma_z\rangle_{ss}\right) - \tilde{\Omega}\,\langle\sigma_x\rangle_{ss}\,. \end{aligned} \tag{7.56}$$

For a resonant driving field we have $\tilde{\Delta} = 0$, and the stationary populations of the dressed states depend solely on $\langle\sigma_x\rangle_{ss}$, which, on the other hand, can be nonzero only when the phase ϕ is different from 0 or π and, simultaneously, there is a nonzero squeezing at the atomic resonance. This suggests that the

best candidate to observe the unequal populations of the dressed states would be a squeezed vacuum produced by a degenerate rather than nondegenerate parametric amplifier. In Fig. 7.3(a) we have plotted the population inversion, $\tilde{\sigma}_z = \rho_{++} - \rho_{--}$, of the dressed states as a function of Ω/γ and Δ/γ for $\phi = \pi/2$, $\kappa/\gamma = 20$, and $\epsilon/\kappa = 0.25$, such that $N(\omega_A) = 1.78$ and $M(\omega_A) = 2.22$. In Fig. 7.3(b) the dependence of the population inversion on Ω/γ and κ/γ is illustrated for $\Delta = 0$ and the other parameters as in figure (a). It is clearly seen that the population inversion can take both positive and negative values. For small values of the Rabi frequency, $\Omega \simeq 0$, a jump is observed in the population difference of the dressed states when the detuning Δ changes its sign, which is a consequence of the fact that for the Rabi frequency going to zero the dressed states (7.54) become the bare atomic states $|g\rangle$ and $e\rangle$, but they are interchanged when Δ changes its sign. A clear maximum appears for small Rabi frequencies. The positive values of the population difference mean actual population inversion of the dressed states, which is evident from Fig. 7.3(a). This effect is an example of a nonsecular effect, which appears only for small Rabi frequencies and/or detunings. The peak vanishes for large Rabi frequencies and/or detunings. The peak in the population inversion is due to squeezing.

We note from Fig. 7.3(b) that for small values of κ/γ the population inversion $\tilde{\sigma}_z$ strongly depends on the squeezing bandwidth. However, the study of this behavior in the regime $\kappa/\gamma < 10$ is forbidden by the Markov approximation made in the derivation of the master equation (7.26), which requires the squeezing bandwidth to be much greater than the atomic linewidth. We believe, however, that for sufficiently large values of the DPO bandwidth, $\kappa/\gamma > 10$, which are still consistent with actual experiments on spectroscopy with squeezed light [26], our master equation leads to reasonable results allowing for studies of squeezing bandwidth effects.

Having available the steady-state populations of the dressed states, we can easily check whether the population trapping effect, predicted by Courty and Reynaud [10] (see also [52]) for a broadband squeezed vacuum, can be observed for a narrow-bandwidth squeezed vacuum. In Fig. 7.4(a) we plot the population ρ_{--} as a function of Ω/γ and Δ/γ for $\phi = \pi$, and the DPO output with $\kappa/\gamma = 10^5$ and $\epsilon/\kappa = 0.25$. In this case the squeezed vacuum is very broad and, as is seen from Fig. 7.4(a), there is a population trapping ($\rho_{--} = 1$). Interestingly, the population trapping appears for very large detunings and Rabi frequencies, indicating that this is essentially a secular effect. Figure 7.4(b) shows the population ρ_{--} for the same parameters as in Fig. 7.4 (a) but for a narrow-bandwidth squeezed vacuum with $\kappa/\gamma = 20$. There is no population trapping for the narrow-bandwidth squeezed vacuum. This shows that some effects known from broadband squeezing do not appear for narrow-bandwidth squeezing.

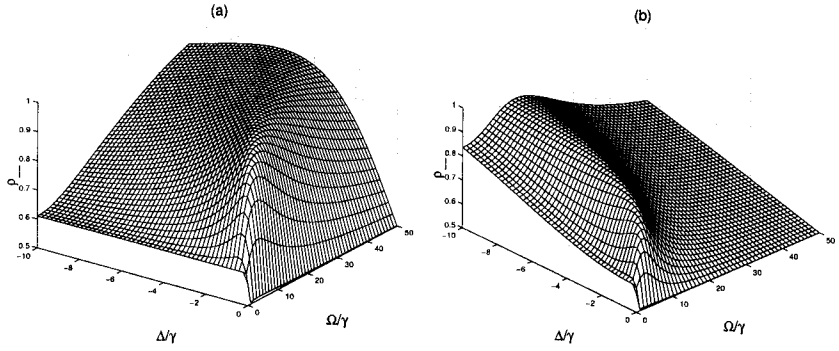

Fig. 7.4 Population ρ_{--} as a function of the detuning Δ and the Rabi frequency Ω, for DPO squeezing with $\epsilon/\kappa = 0.25$, $\phi = \pi$, and (a) $\kappa/\gamma = 10^5$, (b) $\kappa/\gamma = 20$.

Applying the matrix $\mathbf{T}$ to equations (7.40) we arrive at the following evolution equations for the dressed atom quantities

$$\frac{\mathrm{d}}{\mathrm{d}t}\begin{pmatrix}\langle\tilde{\sigma}_-\rangle\\ \langle\tilde{\sigma}_+\rangle\\ \langle\tilde{\sigma}_z\rangle\end{pmatrix} = \tilde{\mathbf{A}}\begin{pmatrix}\langle\tilde{\sigma}_-\rangle\\ \langle\tilde{\sigma}_+\rangle\\ \langle\tilde{\sigma}_z\rangle\end{pmatrix} + \frac{\gamma}{2}\begin{pmatrix}\tilde{\Omega}\\ \tilde{\Omega}\\ 2\tilde{\Delta}\end{pmatrix}, \tag{7.57}$$

where the matrix $\tilde{\mathbf{A}} = \mathbf{T}\mathbf{A}\mathbf{T}^{-1}$ has the following matrix elements:

$$\begin{aligned}
\tilde{A}_{11} &= \tilde{A}^*_{22} = -i\left(\Omega' + \frac{1}{2}\tilde{\Omega}\Lambda_r\right) - \left\{\Gamma + \frac{1}{2}\left[(1-\tilde{\Delta}^2)(\Gamma - \gamma M_r) - \tilde{\Delta}\tilde{\Omega}\Lambda_i\right]\right\},\\
\tilde{A}_{12} &= \tilde{A}^*_{21} = i\left(\gamma\tilde{M}_i + \frac{1}{2}\tilde{\Omega}\Lambda_r\right) - \frac{1}{2}\left[(1-\tilde{\Delta}^2)(\Gamma + \gamma\tilde{M}_r) - \tilde{\Delta}\tilde{\Omega}\Lambda_i\right],\\
\tilde{A}_{13} &= \tilde{A}^*_{23} = \frac{i}{2}\tilde{\Omega}\gamma\tilde{M}_i - \frac{1}{2}\left[\tilde{\Delta}\tilde{\Omega}(\Gamma - \gamma\tilde{M}_r) + (1-\tilde{\Delta}^2)\Lambda_i\right],\\
\tilde{A}_{31} &= \tilde{A}^*_{32} = i\left(\tilde{\Omega}\gamma\tilde{M}_i - \tilde{\Delta}\Lambda_r\right) - \tilde{\Delta}\tilde{\Omega}(\Gamma - \gamma\tilde{M}_r) + \tilde{\Delta}^2\Lambda_i,\\
\tilde{A}_{33} &= -2\left\{\Gamma - \frac{1}{2}\left[(1-\tilde{\Delta}^2)(\Gamma - \gamma\tilde{M}_r) - \tilde{\Delta}\tilde{\Omega}\Lambda_i\right]\right\}.
\end{aligned} \tag{7.58}$$

In the secular approximation, when Ω' is much larger than all the damping rates, the nondiagonal matrix elements of the matrix $\tilde{\mathbf{A}}$ can be omitted and on neglecting also the vector of the free terms, equations (7.57) are decoupled and have simple exponential solutions

$$\langle\tilde{\sigma}_{\pm}(t)\rangle = \langle\tilde{\sigma}_{\pm}(0)\rangle \exp\left\{\pm i\left(\Omega' + \frac{1}{2}\tilde{\Omega}\Lambda_r\right)t - \left[\Gamma + \frac{1}{2}\left[(1-\tilde{\Delta}^2)(\Gamma - \gamma\tilde{M}_r) - \tilde{\Delta}\tilde{\Omega}\Lambda_i\right]\right]t\right\}, \tag{7.59}$$

$$\langle\tilde{\sigma}_z(t)\rangle = \langle\tilde{\sigma}_z(0)\rangle \exp\left\{-2\left[\Gamma - \frac{1}{2}\left[(1-\tilde{\Delta}^2)(\Gamma - \gamma\tilde{M}_r) - \tilde{\Delta}\tilde{\Omega}\Lambda_i\right]\right]t\right\}. \tag{7.60}$$

The solutions (7.59) and (7.60), describing the evolution of the dressed coherences and dressed population inversion, give us immediately some interesting features of the atomic evolution in the secular limit. In particular, it is seen that the Rabi frequency Ω' is shifted by $\tilde{\Omega}\Lambda_r/2$ if the squeezed vacuum has finite bandwidth. The shift is determined by Λ_r, given in (7.30). For resonant fields with $\tilde{\Delta} = 0$, the shift is negligible in the secular limit in which δ_N and δ_M are negligible. However, for nonresonant excitation, $\Delta \neq 0$, the shift is equal to $\tilde{\Omega}\tilde{\Delta}[M(\omega_L) - M(\omega_L + \Omega')]\sin\phi/2$. It is nonzero when the squeezing properties are different at the center and at the sidebands and $\phi \neq 0$ or π. This feature is evidently associated with the finite bandwidth of the squeezed vacuum and disappears for broadband squeezing. From equations (7.59) and (7.60), it is also easy to identify two damping rates:

$$\Gamma_{\text{coh}} = \Gamma + \frac{1}{2}\left[(1-\tilde{\Delta}^2)(\Gamma - \gamma\tilde{M}_r) - \tilde{\Delta}\tilde{\Omega}\Lambda_i\right], \tag{7.61}$$

$$\Gamma_{\text{pop}} = 2\left\{\Gamma - \frac{1}{2}\left[(1-\tilde{\Delta}^2)(\Gamma - \gamma\tilde{M}_r) - \tilde{\Delta}\tilde{\Omega}\Lambda_i\right]\right\}, \tag{7.62}$$

which describe the relaxation of the dressed coherences and populations. For ordinary vacuum, for which $\Gamma = \gamma/2$ and $\tilde{M}_r = \Lambda_i = 0$, the two rates are the well-known expressions [51]. For the broadband squeezed vacuum, for which $M(\omega)$ does not depend on ω and $\Lambda = 0$, the two damping rates are modified with respect to the damping rates for the ordinary vacuum [5, 6]. Since Γ_{coh} is known to determine the width of the sidebands and Γ_{pop} defines the width of the central line of the Mollow triplet, it is seen that the important narrowing of the central line can be observed. This is the well-known effect of the broadband squeezed vacuum [6].

On resonance, $\tilde{\Delta} = 0$, the expressions (7.61) and (7.62) take much simpler form:

$$\begin{aligned}\Gamma_{\text{coh}} &= \frac{1}{2}(\gamma_x + 2\gamma_y), \\ \Gamma_{\text{pop}} &= \gamma_x,\end{aligned} \tag{7.63}$$

where γ_x and γ_y are given by (7.47). This is the result obtained by Yeoman and Barnett [33] showing that the width of the central line is defined by the squeezing present at the sidebands only. The widths of the sidebands depend

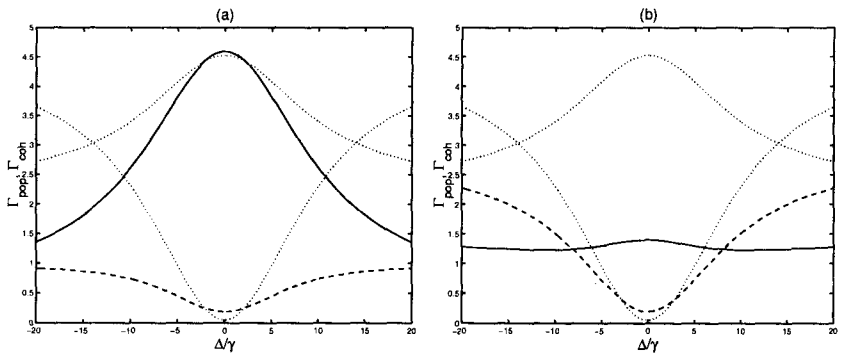

Fig. 7.5 Plots of $\Gamma_{\rm coh}/\gamma$ (solid line) and $\Gamma_{\rm pop}/\gamma$ (dashed line) against Δ for $\kappa/\gamma = 20$, $\epsilon/\kappa = 0.25$, $\Omega/\gamma = 10$, and $\phi = \pi$: (a) DPO and (b) NDPO. Dotted curves present corresponding results for broadband squeezing.

on the squeezing at both the center and the sidebands. Yeoman and Barnett [33] have also shown that for squeezing produced by NDPO, for sufficiently large Rabi frequency, the narrowing of all three spectral components of the Mollow triplet is possible.

Formulas (7.61) and (7.62) are analytical formulas indicating explicitly the modifications of the two damping rates due to squeezed vacuum with finite bandwidth. In Fig. 7.5 we have plotted $\Gamma_{\rm pop}$ and $\Gamma_{\rm coh}$, in units of γ as functions of the detuning Δ for the squeezed vacuum with the bandwidth $\kappa/\gamma = 20$, and for $\epsilon/\kappa = 0.25$, $\Omega/\gamma = 10$, and $\phi = \pi$. Figure 7.5(a) shows the results for DPO and Fig. 7.5(b) for NDPO. The values of $\Gamma_{\rm pop}$ that fall below 0.5 indicate narrowing of the central line of the Mollow triplet. Dotted lines are used to mark the results for broadband squeezing. As it is seen, the narrowing of the central line can be observed for squeezing with $\phi = \pi$ in both DPO and NDPO squeezing. The narrowing is most effective for $\Delta = 0$, and there is no big difference between DPO and NDPO squeezing, at least for the parameters used in Fig. 7.5. It is also seen that the broadband squeezing is more effective in narrowing of the central line than the squeezing with finite bandwidth. The differences between DPO and NDPO are more dramatic for $\Gamma_{\rm coh}$. The sidebands in the squeezing from NDPO are much narrower than those in the squeezing from DPO, and narrower than those in the broadband squeezing, but they do not fall below 0.75, which is the value for the ordinary vacuum. In Fig. 7.6 we illustrate the crucial difference between DPO and NDPO squeezing in narrowing the spectral lines. Figure 7.6(a) shows $\Gamma_{\rm coh}$ and $\Gamma_{\rm pop}$ for DPO squeezing. The narrowing of the central line and broadening of the sidebands are quite evident. In contrast to DPO squeezing, in Fig. 7.6(b) we see the simultaneous narrowing of both the central line and

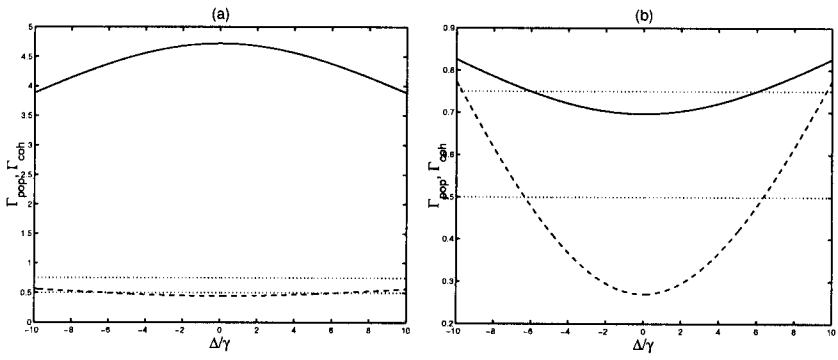

Fig. 7.6 Plots of $\Gamma_{\rm coh}/\gamma$ (solid line) and $\Gamma_{\rm pop}/\gamma$ (dashed line) against Δ for $\kappa/\gamma = 10$, $\epsilon/\kappa = 0.25$, $\phi = \pi$, and $\Omega/\gamma = 20$: (a) DPO and (b) NDPO. Dotted curves mark the results for ordinary vacuum.

the sidebands, in agreement with the Yeoman and Barnett results [33]. The narrowing is most effective for zero detuning.

Of course, formulas (7.61) and (7.62), which give us direct insight into the physical factors defining the widths of the spectral lines, are valid only in the secular limit, when the Rabi frequency is very large in comparison to the atomic linewidth. In this case the dressed atom picture has clear advantage over the standard approach, and equations (7.57) can be decoupled and solved. When the Rabi frequency in not very large, the nonsecular terms can be important, and the dressed atom picture is no longer advantageous over the bare atom picture. However, the master equation (7.26) leading to the Bloch equations (7.44) allows for calculations of the fluorescence spectrum in a general case, without making the secular approximation. The only restriction is the bandwidth of the squeezed vacuum, which must be much larger than the atomic linewidth to justify the Markov approximation.

7.3.4 Fluorescence spectrum

The stationary spectrum of the resonance fluorescence from a two-level atom is given by the Fourier transform of the two-time atomic correlation function as [7, 47]

$$\mathcal{F}(\omega) = \gamma 2\mathrm{Re}\left\{\int_0^\infty \langle\sigma_+(0)\sigma_-(\tau)\rangle_{ss}\, \mathrm{e}^{i(\omega-\omega_L)\tau}\, \mathrm{d}\tau\right\}, \tag{7.64}$$

where Re denotes the real part of the integral. The two-time correlation function appearing in (7.64) can be found from the Bloch equations (7.40) by applying the quantum regression theorem [53]. The equations of motion for

the two-time correlation functions can be written as

$$\frac{\partial}{\partial\tau}\begin{pmatrix}\langle\sigma_+(0)\sigma_-(\tau)\rangle_{ss}\\ \langle\sigma_+(0)\sigma_+(\tau)\rangle_{ss}\\ \langle\sigma_+(0)\sigma_z(\tau)\rangle_{ss}\end{pmatrix} = \mathbf{A}\begin{pmatrix}\langle\sigma_+(0)\sigma_-(\tau)\rangle_{ss}\\ \langle\sigma_+(0)\sigma_+(\tau)\rangle_{ss}\\ \langle\sigma_+(0)\sigma_z(\tau)\rangle_{ss}\end{pmatrix} + \langle\sigma_+\rangle_{ss}\begin{pmatrix}0\\0\\-\gamma\end{pmatrix}, \tag{7.65}$$

where $\mathbf{A}$ is the 3×3 matrix given by (7.41), and the initial values for the correlation functions are

$$\begin{aligned}\langle\sigma_+\sigma_-\rangle_{ss} &= \frac{1}{2}(1+\langle\sigma_z\rangle_{ss}),\\ \langle\sigma_+\sigma_+\rangle_{ss} &= 0,\\ \langle\sigma_+\sigma_z\rangle_{ss} &= -\langle\sigma_+\rangle_{ss}.\end{aligned} \tag{7.66}$$

Taking the Laplace transform of (7.65) we obtain a system of algebraic equations for the transformed variables which can easily be solved. The solution gives us the following formula for the Laplace transform of the correlation function $\langle\sigma_+(0)\sigma_-(\tau)\rangle_{ss}$:

$$F(z) = \frac{1}{d(z)}\left\{-i\langle\sigma_+\rangle_{ss}\frac{\Omega}{2}\frac{\gamma+z}{z}\left(\Gamma+\gamma\tilde{M}+i\delta+z\right) + \frac{1}{2}(1+\langle\sigma_z\rangle_{ss})\left[\frac{\Omega}{2}(\Omega+\Lambda)+(2\Gamma+z)(\Gamma+i\delta+z)\right]\right\}, \tag{7.67}$$

where

$$d(z) = d + z\left[z(4\Gamma+z)+\Omega(\Omega+\Lambda_r)+5\Gamma^2+\delta^2-|\gamma\tilde{M}|^2\right] \tag{7.68}$$

with d given by (7.49), and

$$\langle\sigma_+\rangle_{ss} = \langle\sigma_x\rangle_{ss} - i\langle\sigma_y\rangle_{ss} = i\frac{\Omega}{2d}\gamma\left(\Gamma+\gamma\tilde{M}^*-i\delta\right). \tag{7.69}$$

The Laplace transform (7.67) contains both the coherent and incoherent contributions to the spectrum [7]. The coherent part of the spectrum is the delta function $\delta(\omega-\omega_L)$ centered on the laser frequency, the amplitude of which is defined by the residuum for $z=0$:

$$F_{\rm coh} = \lim_{z\to 0} zF(z) = \frac{\Omega^2}{4d^2}\left|\gamma\left(\Gamma+\gamma\tilde{M}+i\delta\right)\right|^2. \tag{7.70}$$

The incoherent part of the spectrum is then given by

$$\mathcal{F}_{\rm inc}(\omega) = \gamma\, 2{\rm Re}\left\{F_{\rm inc}(z)|_{z=-i(\omega-\omega_L)}\right\}, \tag{7.71}$$

where

$$F_{\rm inc}(z) = F(z) - \frac{1}{z}F_{\rm coh} = \frac{1}{d(z)}\left\{-i\langle\sigma_+\rangle_{ss}\frac{\Omega}{2}\left(\gamma+\Gamma+\gamma\tilde{M}+i\delta+z\right)\right.$$
$$+\frac{1}{2}(1+\langle\sigma_z\rangle_{ss})\left[\frac{1}{2}\Omega(\Omega+\Lambda)+(2\Gamma+z)(\Gamma+i\delta+z)\right]$$
$$\left.-F_{\rm coh}\frac{d(z)-d}{z}\right\}. \tag{7.72}$$

We can relate the incoherent part of the resonance fluorescence spectrum to the quadrature noise spectrum (squeezing spectrum) as [54]

$$\mathcal{F}_{\rm inc}(\omega+\omega_L) = S_X(\omega)+S_Y(\omega)+S_A(\omega), \tag{7.73}$$

where

$$S_X(\omega) = \gamma\,{\rm Re}\int_0^\infty \cos(\omega\tau)\left[\langle\sigma_+(0),\sigma_-(\tau)\rangle_{ss}+\langle\sigma_+(0),\sigma_+(\tau)\rangle_{ss}\right]{\rm d}\tau, \tag{7.74}$$

$$S_Y(\omega) = \gamma\,{\rm Re}\int_0^\infty \cos(\omega\tau)\left[\langle\sigma_+(0),\sigma_-(\tau)\rangle_{ss}-\langle\sigma_+(0),\sigma_+(\tau)\rangle_{ss}\right]{\rm d}\tau, \tag{7.75}$$

are, respectively, in-phase and out-of-phase quadrature components of the noise spectrum, and

$$S_A(\omega) = -2\gamma\int_0^\infty \sin(\omega\tau){\rm Im}\,\langle\sigma_+(0),\sigma_-(\tau)\rangle_{ss}\,{\rm d}\tau \tag{7.76}$$

is the asymmetric contribution to the spectrum. In (7.74)–(7.76), $\langle a,b\rangle \equiv \langle ab\rangle - \langle a\rangle\langle b\rangle$ denotes the covariance.

In order to calculate the spectra of the normally ordered quadrature components of the fluorescent light [55], we need to evaluate the correlation function $\langle\sigma_+(0),\sigma_+(\tau)\rangle_{ss}$, which, on the other hand, can be found from the equations (7.65) and (7.48). The Laplace transform for the function $\langle\sigma_+(0)\sigma_+(\tau)\rangle_{ss}$ has the form

$$S(z) = \frac{1}{d(z)}\left\{i\langle\sigma_+\rangle_{ss}\frac{\Omega}{2}\frac{\gamma+z}{z}\left(\Gamma+\gamma\tilde{M}^*-i\delta+z\right)\right.$$
$$\left.+\frac{1}{2}(1+\langle\sigma_z\rangle_{ss})\left[\frac{\Omega}{2}(\Omega+\Lambda^*)-(2\Gamma+z)\gamma\tilde{M}^*\right]\right\}. \tag{7.77}$$

The components of the squeezing spectra (7.74)–(7.76) are related to the functions $F(z)$ and $S(z)$, given by (7.67) and (7.77), in the following way

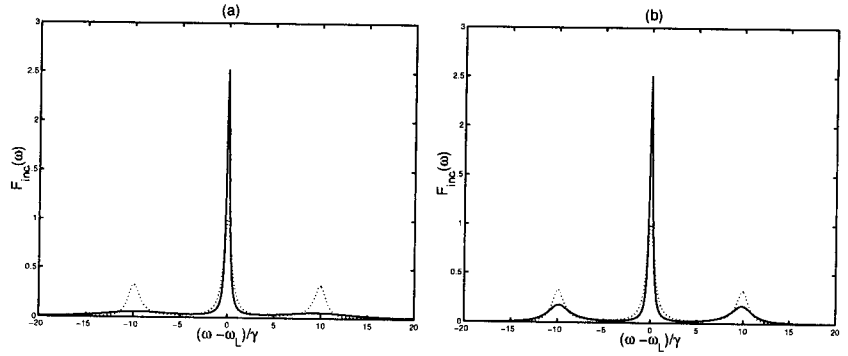

Fig. 7.7 Fluorescence spectrum for $\kappa/\gamma = 20$, $\epsilon/\kappa = 0.25$, $\Omega/\gamma = 20$, $\Delta = 0$, and $\phi = \pi$: (a) DPO and (b) NDPO; Mollow spectrum (dotted line).

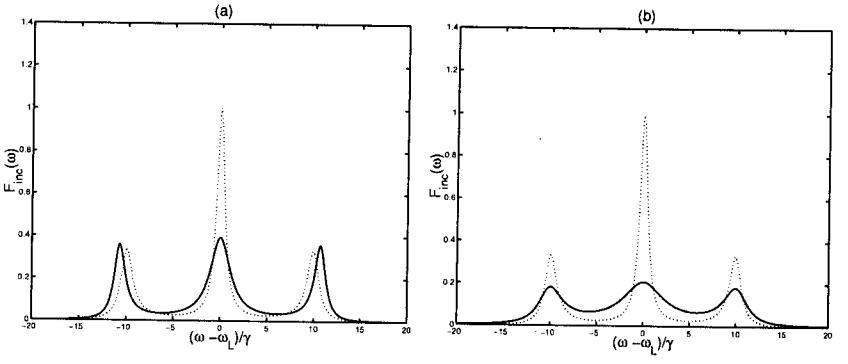

Fig. 7.8 Same as Fig. 7.7 but for $\phi = 0$.

$$
\begin{aligned}
S_X(\omega) &= \frac{1}{4}\,\mathrm{Re}\left\{F(-i\omega) + F(i\omega) + S(-i\omega) + S(i\omega)\right\}, \\
S_Y(\omega) &= \frac{1}{4}\,\mathrm{Re}\left\{F(-i\omega) + F(i\omega) - S(-i\omega) - S(i\omega)\right\}, \qquad (7.78) \\
S_A(\omega) &= \frac{1}{2}\,\mathrm{Re}\left\{F(-i\omega) - F(i\omega)\right\}.
\end{aligned}
$$

In Fig. 7.7 we plot the fluorescence spectrum for $\Delta = 0$, $\Omega/\gamma = 10$, and the squeezed vacuum produced by (a) DPO and (b) NDPO with $\kappa/\gamma = 20$, $\epsilon/\kappa = 0.25$ [$N(\omega_A) = 1.78$, $|M(\omega_A)| = 2.22$], and $\phi = \pi$. The spectrum in the squeezed vacuum is symmetric and contains three peaks, just as does the Mollow spectrum in the normal vacuum [7]. The linewidths of the spectral features, however, are different and can be narrower than those in the normal

vacuum. The narrowing of the central line is clearly visible for both the DPO and NDPO squeezing. The sidebands are broader with respect to the standard Mollow spectrum, but the broadening is less effective for NDPO than for DPO. This confirms our earlier predictions based on the damping rates $\Gamma_{\rm pop}$ and $\Gamma_{\rm coh}$ of the dressed atomic populations and coherences (see Section 7.3.3). In Fig. 7.8 the resonance fluorescence spectra are shown for $\phi = 0$ and other parameters as for Fig. 7.7. In this case, we see that the intensities of the spectral lines are different and we observe a shift of the Rabi sidebands from their resonant positions, which is clearly visible in Fig. 7.8(a). The shift is due to the presence of the parameters δ_N and δ_M which are different from zero *only* in a narrow-bandwidth squeezed vacuum. The shift vanishes when the bandwidth goes to infinity. Therefore, the shift of the Rabi sidebands, seen in Fig. 7.8(a), is a signature of the narrow-bandwidth squeezed vacuum.

To find the positions and widths of the spectral lines of the fluorescence spectrum given by (7.72), it is enough to find eigenvalues of the matrix $\mathbf{A}$ given by (7.41) or, equivalently, find the roots of the third-order polynomial $d(z)$ given by (7.68). It is easy to show that for $\Delta = 0$ and $\phi = 0$ the eigenvalues are

$$\begin{aligned} z_0 &= -\left(\Gamma + \gamma|\tilde{M}_r|\right), \\ z_\pm &= -\frac{1}{2}\left(3\Gamma - \gamma|\tilde{M}_r|\right) \pm i\sqrt{\left(\Omega + \frac{1}{2}\Lambda_r\right)^2 - \frac{1}{4}\left[(\Gamma + \gamma|\tilde{M}_r|)^2 + \Lambda_r^2\right]}. \end{aligned} \tag{7.79}$$

The eigenvalues for $\phi = \pi$ are obtained by changing $|\tilde{M}_r| \to -|\tilde{M}_r|$. It is seen from (7.79) that the spectral linewidths can be narrower than those in the normal vacuum, and for a strong driving field the Rabi sidebands are shifted from $\pm\Omega$ positions to $\pm(\Omega + \frac{1}{2}\Lambda_r)$. According to (7.30), the shift Λ_r depends on the parameters δ_N and δ_M. In the secular limit we can forget the second term under the square root, and the real parts of the roots (7.79) reproduce the damping rates $\Gamma_{\rm coh}$ and $\Gamma_{\rm pop}$, given by (7.61) and (7.62) for $\Delta = 0$ and $\phi = 0$. For strong driving fields there are three lines, as expected, and the incoherent part of the resonance fluorescence spectrum has the simple analytical form [56]

$$\begin{aligned} \mathcal{F}(\omega)/\gamma = F_0 &\frac{\gamma_x}{(\omega - \omega_L)^2 + \gamma_x^2} + \frac{\left(\frac{1}{2}\gamma_x + \gamma_y\right) F_a + (\omega - \omega_L + \Omega_R) F_d}{(\omega - \omega_L + \Omega_R)^2 + \left(\frac{1}{2}\gamma_x + \gamma_y\right)^2} \\ &+ \frac{\left(\frac{1}{2}\gamma_x + \gamma_y\right) F_a - (\omega - \omega_L - \Omega_R) F_d}{(\omega - \omega_L - \Omega_R)^2 + \left(\frac{1}{2}\gamma_x + \gamma_y\right)^2}, \end{aligned} \tag{7.80}$$

where the amplitudes are

$$\begin{aligned} F_0 &= \frac{1}{2}\left(1-\frac{\gamma\gamma_y}{R^2}\right), \\ F_a &= \frac{1}{4}\left(1-\frac{\gamma\gamma_y}{R^2}-\frac{\gamma^2\Omega^2}{R^4}\right), \\ F_d &= \frac{1}{4}\frac{\gamma}{\Omega_R}\left(2\frac{\gamma_x}{\gamma}F_a+\frac{\Omega^2}{R^2}F_0\right), \end{aligned} \tag{7.81}$$

and

$$\Omega_R = \sqrt{\left(\Omega+\frac{1}{2}\Lambda_r\right)^2-\frac{1}{4}\left(\gamma_x^2+\Lambda_r^2\right)}, \tag{7.82}$$

$$R = \sqrt{\Omega_R^2+\left(\frac{1}{2}\gamma_x+\gamma_y\right)^2}, \tag{7.83}$$

where γ_x and γ_y are given by (7.47). The spectrum (7.80) exhibits the Lorentzian line with the amplitude F_0 and the width γ_x at the laser frequency ω_L, and the Lorentzian lines with the width $\gamma_x/2+\gamma_y$ and the amplitude F_a as well as the dispersion features with the amplitude F_d at the sidebands $\omega=\omega_L\pm\Omega_R$. In the secular limit $\Omega\gg\gamma$ we have $\Omega_R\approx R\approx\Omega$, which gives $F_0=1/2$, $F_a=1/4$, and $F_d\approx 0$. This leads to the symmetric three-peak spectrum, but with the widths modified by the squeezed vacuum [6]. Formula (7.80) is valid for strong fields above the threshold $(\Omega+\Lambda_r/2)^2-(\gamma_x^2+\Lambda_r^2)/4>0$. Below the threshold there is no splitting into three lines and the spectrum is composed of three Lorentzian contributions with different widths centered at laser frequency [56]. For moderate fields, above threshold, the amplitudes of the lines are modified and the dispersion feature starts to play a role. For nonzero detuning and $\phi\neq 0$ the general formulas (7.71) and (7.72) can be applied, and we have used them to plot the spectra.

Another interesting feature appears for a weak driving field. In Fig. 7.9 we plot the fluorescence spectrum for $\Omega/\gamma=0.2$, $\Delta=0$, $\kappa/\gamma=20$, and different ϵ/γ. In this case we fix the bandwidth of the DPO cavity and change the pumping rate ϵ which determines the intensity of the squeezed vacuum. Here we see that the spectrum is composed of a single peak which exhibits a hole for small ϵ. The hole burning in the spectrum was first predicted by Swain [57] for a broadband squeezed vacuum and interpreted as arising from the presence of squeezing in the fluorescence field [54]. Figure 7.9 shows that the effect also appears for a narrow-bandwidth squeezed vacuum, as shown in [37]. The origin of the hole is the squeezing in the fluorescence field. In Fig. 7.10 we plot the noise quadratures $S_X(\omega)$ and $S_Y(\omega)$ together with the asymmetric part $S_A(\omega)$. The $S_Y(\omega)$ component is negative, indicating squeezing in the emitted fluorescence field. Thus, the hole in the spectrum results from the

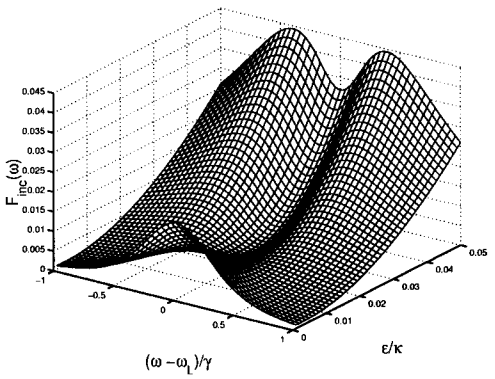

Fig. 7.9 Fluorescence spectrum for DPO with $\kappa/\gamma = 20$, $\Omega/\gamma = 0.2$, $\Delta = 0$, and $\phi = 0$.

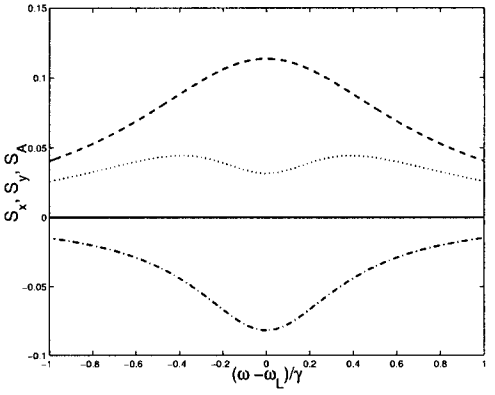

Fig. 7.10 Squeezing spectra for DPO with $\epsilon/\kappa = 0.05$ and other parameters as in Fig. 7.9. The dotted line is the fluorescence spectrum.

presence of squeezing in the fluorescence field. It is well known that in this regime of the parameters, a two-level atom produces squeezed light even in the absence of the squeezed vacuum [58], and there is no hole in the spectrum. However, the squeezing produced in this way is too weak to burn a hole in the spectrum. The presence of the external squeezed vacuum field leads to an enhancement of the squeezing in the fluorescence field.

Apart from the narrowing of the spectral lines and the hole burning, the fluorescence spectrum can exhibit asymmetries in the intensities of the spectral lines. In Fig. 7.11(a) we plot the fluorescence spectrum for $\Omega/\gamma = 3$, $\Delta = 0$, $\phi = \pi/2$ and the DPO parameters $\kappa/\gamma = 20$, $\epsilon/\gamma_c = 0.125$. In this

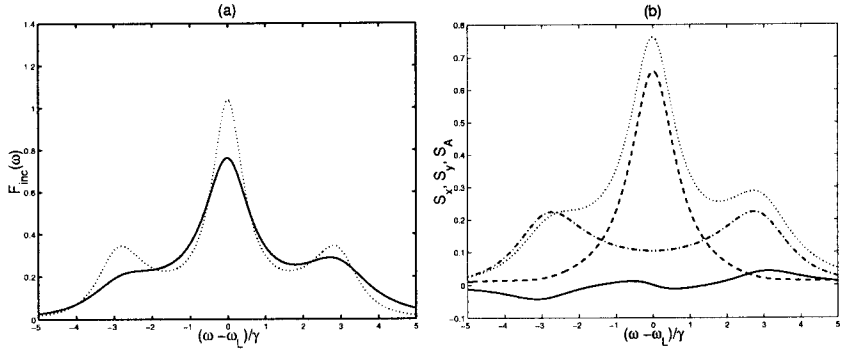

Fig. 7.11 (a) Fluorescence spectrum for DPO with $\kappa/\gamma = 20$, $\epsilon/\kappa = 0.125$, $\Omega/\gamma = 3$, $\Delta = 0$, and $\phi = \pi/2$; Mollow spectrum (dotted line). (b) Squeezing spectra $S_X(\omega)$ (dashed line), $S_Y(\omega)$ (dashed-dotted line) and the asymmetric part $S_A(\omega)$ (solid line); fluorescence spectrum (dotted line).

case the spectrum is not symmetric despite the fact that the atom is driven by a resonant laser field. The asymmetry arises from the unequal populations of the dressed states, discussed in Section 7.3.3. In Fig. 7.11(b) we plot the noise components $S_X(\omega)$ and $S_Y(\omega)$ together with the asymmetric part $S_A(\omega)$. Now, the noise components are both positive and symmetric. The asymmetric part, however, is different from zero and exhibits a negative peak at the lower-frequency Rabi sideband. The negative peak in $S_A(\omega)$ can be interpreted as arising from a stimulated emission between the dressed states induced by the squeezed vacuum.

The role of the asymmetric part is more dramatic when one considers the fluorescence spectrum for an off-resonant driving field. In Fig. 7.12 we plot the fluorescence spectrum as a function of $(\omega - \omega_L)/\gamma$ and ϵ/κ for $\Omega/\gamma = 5$, $\Delta/\gamma = -5$, $\phi = \pi$ and a fixed bandwidth $\kappa/\gamma = 20$ of (a) DPO and (b) NDPO. For small ϵ the high-frequency Rabi sideband and the central peak can be suppressed. As ϵ increases the central peak and the high-frequency Rabi sideband emerge and simultaneously the low-frequency Rabi sideband disappears. In general, the spectrum is asymmetric for a large range of ϵ. Inspection of the noise spectrum $S_X(\omega) + S_Y(\omega)$ indicates that there are positive peaks at the frequencies at which there are no fluorescence peaks. Therefore, according to (7.73), the asymmetry is produced by the $S_A(\omega)$ part. This is shown in Fig. 7.13, where we plot the noise spectra. Here, there is no squeezing in the fluorescence field and the suppression of the lower-frequency Rabi sideband comes from the asymmetric term, $S_A(\omega)$. The noise peaks and the asymmetric part reveal processes which are averaged to zero in the fluorescence spectrum. At this frequency we have absorption of photons by the squeezed vacuum followed by spontaneous emission. Thus, although there

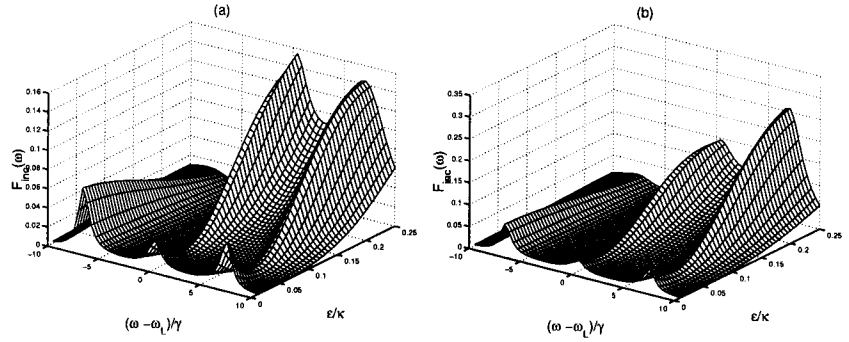

Fig. 7.12 Fluorescence spectrum for $\kappa/\gamma = 20$, $\Omega/\gamma = 5$, $\Delta/\gamma = -5$, and $\phi = \pi$: (a) DPO squeezing, (b) NDPO squeezing.

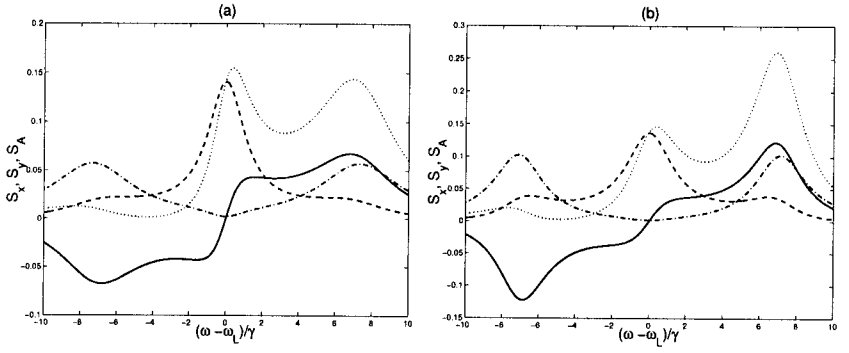

Fig. 7.13 Squeezing spectra $S_X(\omega)$ (dashed line), $S_Y(\omega)$ (dashed-dotted line) and the asymmetric part $S_A(\omega)$ (solid line) for (a) DPO squeezing and (b) NDPO squeezing with $\epsilon/\gamma = 0.25$ and other parameters as in Fig. 7.12; fluorescence spectrum (dotted line).

is no lower Rabi sideband in the fluorescence spectrum, there is a significant amount of noise at this frequency, as shown in the noise spectrum. It therefore follows that at frequencies of zero fluorescence, the absorption and emission cancel each other. The changes are less dramatic in case of NDPO, but they appear for both DPO and NDPO.

7.3.5 Absorption spectrum

Another spectroscopic feature accessible to experimental verification is the probe absorption spectrum. The probe absorption spectrum of a two-level atom is given by the Fourier transform of the two-time atomic correlation

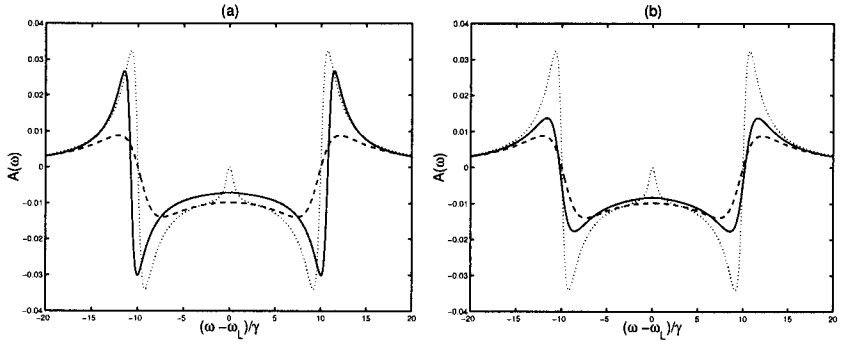

Fig. 7.14 Absorption spectrum for $\epsilon/\kappa = 0.25$, $\Delta/\gamma = 0$, $\Omega/\gamma = 10$, and $\phi = 0$: finite bandwidth (solid line), broadband squeezing (dashed line), and no squeezing (dotted line). (a) DPO and (b) NDPO.

functions as [14]

$$\mathcal{A}(\omega) = \gamma\, 2\mathrm{Re}\left\{\int_0^\infty \langle[\,\sigma_-(\tau),\sigma_+(0)]\rangle_{ss}\, \mathrm{e}^{i(\omega-\omega_L)\tau}\,\mathrm{d}\tau\right\}, \tag{7.84}$$

where Re denotes the real part of the integral. The absorption spectrum is defined by the difference of two atomic correlation functions [coming from the commutator in (7.84)]. The evolution of such a difference can be found from the Bloch equations (7.40) by applying the quantum regression theorem [53]. The equations of motion for the difference of two-time correlation functions can be written as

$$\frac{\partial}{\partial\tau}\begin{pmatrix} \langle[\sigma_-(\tau),\sigma_+(0)]\rangle_{ss} \\ \langle[\sigma_+(\tau),\sigma_+(0)]\rangle_{ss} \\ \langle[\sigma_z(\tau),\sigma_+(0)]\rangle_{ss} \end{pmatrix} = \mathbf{A}\begin{pmatrix} \langle[\sigma_-(\tau),\sigma_+(0)]\rangle_{ss} \\ \langle[\sigma_+(\tau),\sigma_+(0)]\rangle_{ss} \\ \langle[\sigma_z(\tau),\sigma_+(0)]\rangle_{ss} \end{pmatrix}, \tag{7.85}$$

where $\mathbf{A}$ is the 3×3 matrix given by (7.41), and the initial values for the correlation functions are

$$\begin{aligned} \langle\sigma_-\sigma_+\rangle_{ss} - \langle\sigma_+\sigma_-\rangle_{ss} &= -\langle\sigma_z\rangle_{ss}\,, \\ \langle\sigma_+\sigma_+\rangle_{ss} &= 0\,, \\ \langle\sigma_z\sigma_+\rangle_{ss} - \langle\sigma_+\sigma_z\rangle_{ss} &= 2\,\langle\sigma_+\rangle_{ss}\,. \end{aligned} \tag{7.86}$$

Taking the Laplace transform of (7.85) we obtain the system of algebraic equations for the transformed variables, which can easily be solved. The solution gives us the following formula for the Laplace transform of the difference

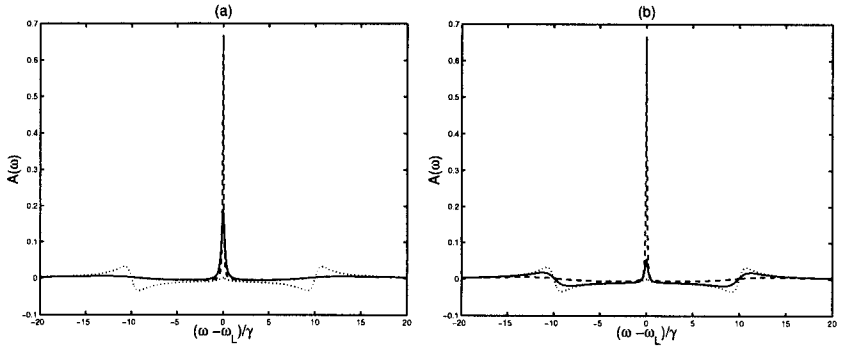

Fig. 7.15 Same as Fig. 7.14 but for $\phi = \pi$.

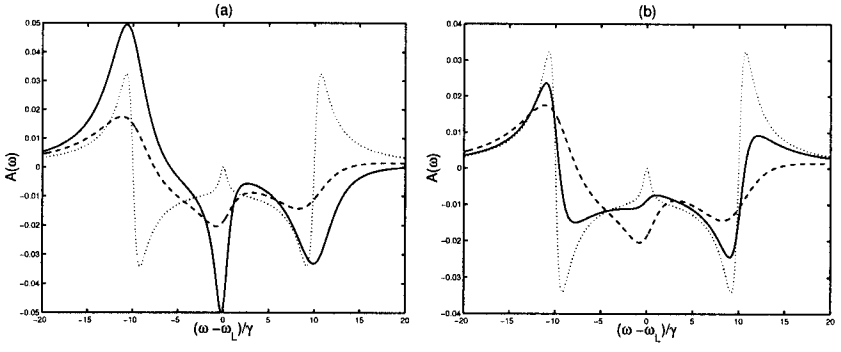

Fig. 7.16 Same as Fig. 7.14 but for $\phi = \pi/2$.

$\langle \sigma_-(\tau)\sigma_+(0)\rangle_{ss} - \langle \sigma_+(0)\sigma_-(\tau)\rangle_{ss}$:

$$A(z) = \frac{1}{d(z)}\left\{ i\langle\sigma_+\rangle_{ss}\,\Omega\left(\Gamma + \gamma\tilde{M} + i\delta + z\right) - \langle\sigma_z\rangle_{ss}\left[\frac{\Omega}{2}(\Omega + \Lambda) + (2\Gamma + z)(\Gamma + i\delta + z)\right]\right\}, \tag{7.87}$$

where $d(z)$ is the same as (7.68) with d given by (7.49), and $\langle\sigma_+\rangle_{ss}$ is given by (7.69).

From the Laplace transform (7.87), the probe absorption spectrum defined by (7.84) is obtained as

$$\mathcal{A}(\omega) = \gamma\, 2\mathrm{Re}\{A(z)|_{z=-i(\omega-\omega_L)}\}. \tag{7.88}$$

Formulas (7.87) and (7.88) give pretty simple analytical expressions that describe the probe absorption spectrum of the atom driven by the external field with the Rabi frequency Ω, detuned by Δ from the atomic resonance, and damped to the finite bandwidth squeezed vacuum. In the case of a strong field, for $\Delta = 0$ and $\phi = 0$ or $\phi = \pi$, the roots (7.79) can be used to find simple analytical formulas for the probe absorption spectra [59]. The analytical form of the probe absorption spectrum $\mathcal{A}(\omega)/\gamma$ has the same structure as the resonance fluorescence spectrum given by equation (7.80), but with the amplitudes F_0, F_a, and F_d replaced by A_0, A_a, and A_d given by the formulas

$$A_0 = \frac{\gamma\gamma_y}{R^2}, \quad A_a = \frac{1}{2}A_0, \quad A_d = \frac{1}{4}\frac{\gamma}{\Omega_R}\left(2\frac{\Omega^2}{R^2} - \frac{\gamma_x(\gamma_x+\gamma_y)}{R^2}\right). \tag{7.89}$$

For large Rabi frequency Ω, the amplitudes A_0 and A_a are of the order of Ω^{-2}, and the amplitude $A_d \sim \Omega^{-1}$ is the dominant term in the spectrum. This means that the absorption spectrum shows dispersion features at the sidebands.

In general, formulas (7.87) and (7.88) should be used to calculate absorption spectra. Examples of the probe absorption spectra, in units of γ, for the DPO and NDPO squeezing into which the atom is coupled are shown in Figs. 7.14 to 7.16. It is seen that the absorption spectra depend strongly on the phase of squeezing. The negative values of the absorption spectrum mean amplification of the probe signal. For a strong field, $\Omega/\gamma = 10$, there are two dispersion profiles at the sidebands, which are modified strongly by the squeezed vacuum, but generally the finite bandwidth of the squeezed vacuum reservoir leads to smoother profiles than those for broadband squeezing.

7.4 ATOM DRIVEN BY A SQUEEZED VACUUM: COUPLED-SYSTEMS APPROACH

When the squeezed vacuum is treated as a reservoir to the atom, as in Sec. 7.3, the bandwidth of the squeezed vacuum must be much broader than the atomic linewidth to satisfy conditions for the Markov approximation made to derive the master equation (7.26). Another possibility that allows for calculations of the effects of finite squeezing bandwidth is provided by the coupled-systems approach [38]. In this approach one considers a quantum system consisting of two subsystems. A field $b_{\text{in}}(1,t)$ drives the first system and give rise to an output $b_{\text{out}}(1,t)$ which, after a propagation delay τ, becomes the input field $b_{\text{in}}(2,t)$ to the second system. In our case the first system is a degenerate parametric oscillator (DPO) the output of which drives a two-level atom, as shown in Fig. 7.17. In the coupled-systems approach it is assumed that the output from the first system drives the second system without there being any coupling back from the second system to the first, which experimentally

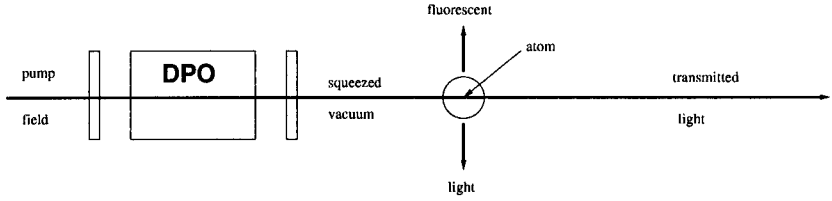

Fig. 7.17 Schematic diagram of the coupled systems

can be achieved by appropriate isolation techniques. Such a one-way coupling can be described in terms of an appropriately chosen Hamiltonian [3].

In our case of driving the atom by a squeezed field generated by DPO, the Hamiltonian can be written in the form [38]

$$H = H_{\rm sys} + H_B + H_{\rm int}\,, \tag{7.90}$$

where

$$\begin{aligned} H_{\rm sys} &= \hbar\omega_s a^\dagger a + \frac{i\hbar}{2}\left(\epsilon a^{\dagger 2}\mathrm{e}^{-i2\omega_s t} - \epsilon^* a^2 \mathrm{e}^{i2\omega_s t}\right) \\ &\quad + \frac{1}{2}\hbar\omega_A\sigma_z + \frac{1}{2}\hbar\Omega\left(\sigma_+\mathrm{e}^{-i\omega_l t} + \sigma_-\mathrm{e}^{i\omega_L t}\right)\,, \qquad (7.91) \\ H_B &= \hbar\int_{-\infty}^{\infty} |\omega|\, b^\dagger(\omega)\, b(\omega)\,\mathrm{d}\omega\,, \qquad (7.92) \\ H_{\rm int} &= i\hbar\int_{-\infty}^{\infty} K_1(\omega)\left[b^\dagger(\omega)\, a - a^\dagger\, b(\omega)\right]\,\mathrm{d}\omega \\ &\quad + i\hbar\int_{-\infty}^{\infty} K_2(\omega)\left[\sigma_- b^\dagger(\omega)\mathrm{e}^{-i\omega\tau} - \sigma_+ b(\omega)\mathrm{e}^{i\omega\tau}\right]\,\mathrm{d}\omega\,. \qquad (7.93) \end{aligned}$$

The system Hamiltonian (7.91) describes the cavity mode at frequency ω_s, which is pumped nonlinearly by a classical field with amplitude ϵ and frequency $2\omega_s$, which consists of the degenerate parametric oscillator (the first system of the two coupled systems), and the two-level atom with the transition frequency ω_A (the second system). The atom is additionally pumped by a classical driving field with the Rabi frequency Ω. In equations (7.92) and (7.93), the operators $b(\omega)$ and $b^\dagger(\omega)$ are the boson annihilation and creation operators for the bath, $K_1(\omega)$ describes the coupling of the cavity mode to the bath, and $K_2(\omega)$ describes the coupling of the atom to the bath.

The Hamiltonian (7.90) leads to the following equation of motion for the bath operator $b(\omega)$:

$$\dot{b}(\omega,t) = -i\,|\omega|\, b(\omega,t) + K_1(\omega)a + K_2(\omega)\sigma_-(t)\mathrm{e}^{-i\omega\tau}. \tag{7.94}$$

For any system operator A, i.e., any operator in the Hilbert space of either the DPO or the two-level atom, one gets the equation of motion

$$\begin{aligned}\dot{A} &= -\frac{i}{\hbar}[A, H_{\rm sys}] + \int K_1(\omega)\,\{b^\dagger(\omega,t)[a,A] - [a^\dagger,A]\,b(\omega,t)\}\,\mathrm{d}\omega \\ &\quad + \int K_2(\omega)\,\{b^\dagger(\omega,t)[\sigma_-,A] - [\sigma_+,A]\,b(\omega,t)\}\,\mathrm{d}\omega. \end{aligned} \tag{7.95}$$

After formally integrating equation (7.94) and substituting the result to equation (7.95), we arrive at the quantum Langevin equation

$$\begin{aligned}\dot{A} &= -\frac{i}{\hbar}[A, H_{\rm sys}] - [A,a^\dagger]\left\{\frac{\gamma_1}{2}\,a + \sqrt{\gamma_1}\,b_{\rm in}(t)\right\} \\ &\quad + \left\{\frac{\gamma_1}{2}\,a^\dagger + \sqrt{\gamma_1}\,b_{\rm in}^\dagger(t)\right\}[A,a] \\ &\quad - [A,\sigma_+]\left\{\frac{\gamma_1}{2}\,\sigma_- + \sqrt{\gamma_1\gamma_2}\,a(t-\tau) + \sqrt{\gamma_2}\,b_{\rm in}(t-\tau)\right\} \\ &\quad + \left\{\frac{\gamma_2}{2}\,\sigma_+ + \sqrt{\gamma_1\gamma_2}\,a^\dagger(t-\tau) + \sqrt{\gamma_2}\,b_{\rm in}(t-\tau)\right\}[A,\sigma_-], \end{aligned} \tag{7.96}$$

where $\gamma_1 = 2\pi K_1^2(\omega_s)$ and $\gamma_2 = 2\pi K_2^2(\omega_s)$. The input–output relations give

$$b_{\rm out}(1,t) = b_{\rm in}(1,t) + \sqrt{\gamma_1}\,a(t), \tag{7.97}$$

$$b_{\rm in}(2,t) = b_{\rm out}(1,t-\tau) + \sqrt{\gamma_1}\,a(t-\tau), \tag{7.98}$$

with

$$b_{\rm in}(t) = b_{\rm in}(1,t) = \frac{1}{\sqrt{2\pi}}\int \mathrm{e}^{-i|\omega|(t-t_0)} b_0(\omega)\,\mathrm{d}\omega\,. \tag{7.99}$$

The quantum Langevin equation (7.96) shows that the evolution of the atomic operators is shifted in time by τ with respect to evolution of the DPO operators. The one-way character of the coupling allows for the separation of the two evolutions, and because τ represents only the shift of the origin of the time for the second system (atom), it can be chosen arbitrarily, and it is convenient to chose $\tau = 0$. This is, however, possible only because of the one-way nature of the coupling.

Assuming that the input field $b_{\rm in}$ is in the vacuum state, we can derive the Ito white noise quantum stochastic differential equation [38, 60]

$$\begin{aligned}\mathrm{d}A &= -\frac{i}{\hbar}\,[A, H_{\rm sys}]\,\mathrm{d}t - \left\{\frac{\gamma_1}{2}\,\left([A,a^\dagger]\,a - a^\dagger\,[A,a]\right)\right. \\ &\quad + [A,\sigma_+]\left(\frac{\gamma_2}{2}\sigma_- + \sqrt{\gamma_1\gamma_2}\,a\right) \\ &\quad \left. - \left(\frac{\gamma_2}{2}\,\sigma_+ + \sqrt{\gamma_1\gamma_2}\,a^\dagger\right)[A,\sigma_-]\right\}\mathrm{d}t \\ &\quad - [A,a^\dagger]\,\mathrm{d}B(t) + \mathrm{d}B^\dagger(t)\,[A,a] \\ &\quad - [A,\sigma_+]\,\mathrm{d}B(t) + \mathrm{d}B^\dagger(t)\,[A,\sigma_-], \end{aligned} \tag{7.100}$$

with

$$\begin{aligned} \mathrm{d}B^\dagger(t)\mathrm{d}B(t) &= [\mathrm{d}B(t)]^2 = 0\,, \\ \mathrm{d}B(t)\mathrm{d}B^\dagger(t) &= \mathrm{d}t\,. \end{aligned} \tag{7.101}$$

The Ito quantum stochastic differential equation (7.100) is equivalent to the following master equation, which in the frame rotating with the squeezed field frequency ω_s has the form

$$\begin{aligned} \dot{\rho} = & \frac{1}{2}[i\Delta\sigma_z + (\epsilon a^{\dagger 2} - \epsilon^* a^2) + \Omega(\sigma_+ + \sigma_-), \rho] \\ & + \frac{\kappa}{2}\{2\,a\rho\,a^\dagger - \rho\,a^\dagger\,a - a^\dagger\,a\rho\} \\ & + \frac{\gamma}{2}\{2\,\sigma_-\rho\,\sigma_+ - \rho\,\sigma_+\,\sigma_- - \sigma_+\,\sigma_-\rho\} \\ & - \sqrt{\eta\kappa\gamma}\,\{[\sigma_+, a\,\rho] + [\rho\,a^\dagger, \sigma_-]\}\,, \end{aligned} \tag{7.102}$$

where $\Delta = \omega_s - \omega_A = \omega_L - \omega_A$ is the detuning of the squeezing carrier frequency (we assume that $\omega_s = \omega_L$) from the atomic resonance, $\gamma_1 = \kappa$ is the DPO cavity bandwidth and $\gamma_2 = \gamma$ is the natural atomic linewidth. The parameter η $(0 < \eta \leq 1)$ describes the matching of the incident squeezed vacuum to the modes surrounding the atom. For perfect matching $\eta = 1$, whereas $\eta < 1$ for an imperfect matching, which is always the case in experimental situations [25, 26, 61]. In order to observe the effects of the squeezed vacuum on the atom, the parameter η should be as close to unity as possible. This requirement could be difficult to achieve in experiments, although some schemes involving optical cavities have been proposed [35, 62]. On the other hand, if the fluorescent field radiated by the atom to the nonsqueezed modes is to be observed, η cannot be exactly unity because the radiation rate to the nonsqueezed modes, which is $(1-\eta)\gamma$, would be zero and no fluorescence would be observed. In the coupled-systems approach one has a choice of detecting either transmitted light or the fluorescent light radiated by the atom to the modes of the ordinary vacuum. The transmitted light is a superposition of the squeezed vacuum coming from the DPO and the field radiated by the atom to the modes occupied by the squeezed vacuum.

7.4.1 Optical spectra for transmitted and fluorescent fields

Effective numerical solutions of the master equation (7.102) are possible when the mean number of photons $\langle a^\dagger a\rangle$ in the cavity is small ($\langle a^\dagger a\rangle < 1$) [38, 63]. In this case it is sufficient to take about ten lowest photon states as a basis of the photon Hilbert space and the two atomic states that form the atomic Hilbert space. Steady-state solutions of the master equation (7.102) together with the quantum regression theorem have been used [41] to find optical spectra for the transmitted and fluorescent fields as well as atomic quadrature noise

spectra for the atom driven by the squeezed vacuum only, when squeezing bandwidth is smaller or comparable to the natural atomic linewidth. In this section we assume that there is no coherent field driving the atom ($\Omega = 0$).

The transmitted field can be described by the (collapse) operator [4, 64]

$$C = \sqrt{\kappa}\, a + \sqrt{\eta\gamma}\, \sigma_- , \tag{7.103}$$

which is a superposition of the incident squeezed vacuum field and the field radiated by the atom into the squeezed field modes. The rate of the atomic radiation that goes to the squeezed modes is equal to $\eta\gamma$, and the fraction $(1-\eta)\gamma$ of the radiation that goes to the remaining (ordinary vacuum) modes constitutes the resonance fluorescence. The photon flux of the transmitted light is given by

$$\langle C^\dagger C\rangle_{ss} = \kappa\langle a^\dagger a\rangle_{ss} + \eta\gamma\langle\sigma_+\sigma_-\rangle_{ss} + \sqrt{\eta\kappa\gamma}\langle a^\dagger\sigma_- + \sigma_+ a\rangle_{ss} , \tag{7.104}$$

and the flux of fluorescent photons that goes to the ordinary vacuum modes is $(1-\eta)\gamma\langle\sigma_+\sigma_-\rangle_{ss}$, where $\langle\cdots\rangle_{ss}$ denotes the steady-state mean value. The total flux is thus

$$\begin{aligned}\langle C^\dagger C\rangle_{ss} + (1-\eta)\gamma\langle\sigma_+\sigma_-\rangle_{ss} \;&=\; \kappa\langle a^\dagger a\rangle_{ss} + \gamma\langle\sigma_+\sigma_-\rangle_{ss} \\ &\quad + \sqrt{\eta\kappa\gamma}\langle a^\dagger\sigma_- + \sigma_+ a\rangle_{ss} .\end{aligned} \tag{7.105}$$

Since the photon flux incident on the atom is $\kappa\langle a^\dagger a\rangle_{ss}$, the last two terms in (7.105) must cancel each other to conserve the energy. This means that the steady-state correlations between the cavity field and atomic operators play an important role in the process.

The steady-state spectrum of the transmitted field can be defined as the Fourier transform of the correlation function

$$\mathcal{T}(\omega) = 2\mathrm{Re}\left\{\int_0^\infty \langle C^+(0)\,, C(\tau)\rangle_{ss} \mathrm{e}^{i(\omega-\omega_s)\tau}\mathrm{d}\tau\right\} , \tag{7.106}$$

where Re denotes the real part of the integral, ω_s is the carrier frequency of the squeezed vacuum field, and we use the notation in which $\langle a, b\rangle \equiv \langle ab\rangle - \langle a\rangle\langle b\rangle$ denotes the covariance, as before.

The incoherent part of the stationary spectrum of resonance fluorescence from a two-level atom is given by the Fourier transform of the two-time atomic correlation function, as defined by (7.64), except for the fact that the rate γ should be replaced by the rate $(1-\eta)\gamma$ because only a fraction $(1-\eta)$ of the total rate is radiated to the ordinary vacuum modes contributing to the resonance fluorescence. Similarly to (7.73), we can relate the incoherent part of the resonance fluorescence spectrum to the quadrature noise spectrum (squeezing spectrum) [54, 65].

The squeezing spectra for the transmitted field can be defined in a similar way by replacing σ_- and σ_+ operators by C and $C^\dagger$ operators and omitting the factor $(1-\eta)\gamma$.

Integrating the squeezing spectrum components over all frequencies gives the variances of the total fluorescence field:

$$F_X = (1-\eta)\gamma \left[\langle\sigma_+\sigma_-\rangle_{ss} - |\langle\sigma_+\rangle_{ss}|^2 - \langle\sigma_+\rangle_{ss}^2\right], \tag{7.107}$$

$$F_Y = (1-\eta)\gamma \left[\langle\sigma_+\sigma_-\rangle_{ss} - |\langle\sigma_+\rangle_{ss}|^2 + \langle\sigma_+\rangle_{ss}^2\right]. \tag{7.108}$$

Squeezing in the total fluorescence field is defined by the requirement that either F_X or F_Y is negative, which can happen only if the stationary atomic dipole moment $\langle\sigma_+\rangle_{ss}$ is different from zero. For a two-level atom driven by the output of a DPO the atomic dipole moment $\langle\sigma_+\rangle_{ss} = 0$ is independent of the parameters used, indicating that the total field variances F_X and F_Y are always positive. It follows that the total fluorescence field does not exhibit squeezing. Nevertheless, it has been shown [37] that even in this case there is a strong squeezing possible in the squeezing spectrum.

Gardiner and Parkins [38] have solved numerically the master equation (7.102) and have found that the squeezing-induced line narrowing in the fluorescence spectrum appears only for the cavity linewidths κ sufficiently large with respect to the atomic natural linewidth γ. The narrowing decreases with decreasing κ and disappears for $\kappa \approx \gamma$. Here, we present optical spectra of the transmitted and fluorescent fields for the case when the cavity damping rate κ is smaller than the atomic natural linewidth [41]. In Fig. 7.18(a) we present the optical spectra of the fluorescent field and the transmitted field for the resonant case $\Delta = 0$, $\kappa/\gamma = 0.35$, the pump field $\epsilon/\kappa = 1/6$ and $\eta = 0.9$. We see that the resonance fluorescence spectrum exhibits a three-peak structure and there is a hole at the center of the transmitted light spectrum. For reference, we plot the Lorentzian with the atomic linewidth $\gamma = 1$ (broader) and the Lorentzian with the linewidth κ (narrower). One can see that the fluorescence spectrum has two components: the broad background with the natural linewidth at the wings and the narrow peak with the width narrower than κ at the center. The appearance of the unusual features in the spectra can be explained as arising from the squeezing produced by the atom. This is seen from Fig. 7.18(b), where we plot the squeezing spectra for the fluorescent field defined by (7.74) and (7.75). The $S_Y(\omega)$ quadrature is negative for frequencies near the carrier frequency ω_s; i.e., it shows squeezing near the center of the spectrum [55, 66]. This squeezing is responsible for the unusual shape of the resonance fluorescence spectrum.

The $S_X(\omega)$ quadrature is positive, and the adding of two squeezing spectra gives the fluorescence spectrum. Clearly, the hole burning arises from squeezing in the fluorescence field and an experimental observation of the effect could be a manifestation of the quantum nature of squeezed light.

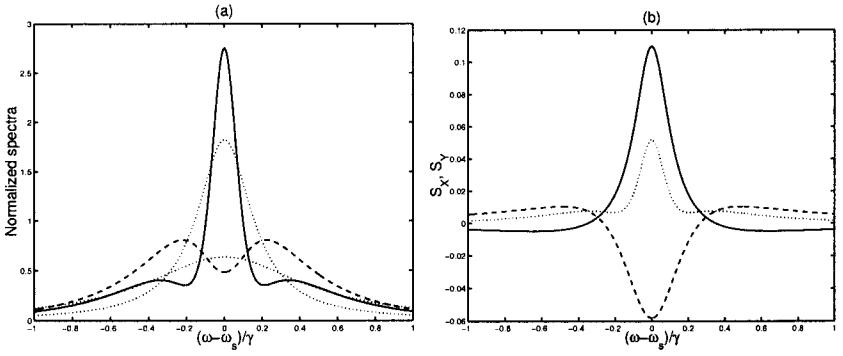

Fig. 7.18 (a) Resonance fluorescence (solid line) and transmitted field (dashed line) spectrum; the dotted lines are two Lorentzians with linewidths γ and κ. (b) Squeezing spectra $S_X(\omega)$ (solid line) and $S_Y(\omega)$ (dashed line); the dotted line is the resonance fluorescence. The values of the parameters are: $\kappa/\gamma = 0.35$, $\epsilon/\kappa = 1/6$, $\eta = 0.9$.

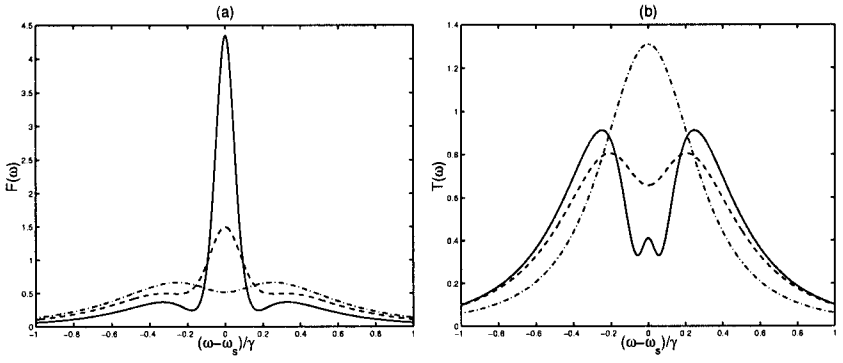

Fig. 7.19 (a) Resonance fluorescence and (b) transmitted field spectra for DPO with $\epsilon/\kappa = 0.1$, $\eta = 0.9$, and $\kappa/\gamma = 0.25$ (solid line), $\kappa/\gamma = 0.5$ (dashed line), and $\kappa/\gamma = 1$ (dashed-dotted line).

In Fig. 7.19 we present both the resonance fluorescence and transmitted field spectra for $\epsilon/\kappa = 1/10$, $\eta = 0.9$, and different κ. The spectrum changes its structure as κ increases. The features discussed here depend crucially on the value of η, which should be as close to unity as possible to have the coupling between the two subsystems as high as possible. On the other hand, there is only a fraction $(1 - \eta)\gamma$ of the radiation that goes to the modes different from the squeezed vacuum modes, and this rate must be nonzero to observe resonance fluorescence to the nonsqueezed modes. In our calculations presented in Figs. 7.18 and 7.19 we have assumed that $\eta = 0.9$. The features,

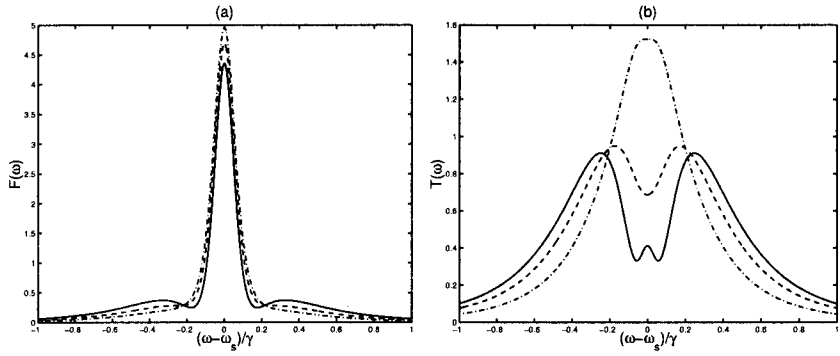

Fig. 7.20 (a) Resonance fluorescence and (b) transmitted field spectra for DPO with $\epsilon/\kappa = 0.1$, $\kappa/\gamma = 0.25$, and $\eta = 0.9$ (solid line), $\eta = 0.7$ (dashed line), $\eta = 0.5$ (dashed-dotted line).

however, degrade quickly as η decreases and disappear for $\eta \approx 0.5$. This is shown in Fig. 7.20, where we plot the fluorescent and transmitted field spectra for different values of η.

7.5 COMPARISON OF THE TWO APPROACHES

In Section 7.4.1 we have presented some unusual features of the resonance fluorescence spectra as well as transmitted spectra that can be observed when the atom is driven by a squeezed vacuum produced by DPO without any coherent driving field. The two approaches presented so far have been applied in the nonoverlapping ranges of the parameters: the master equation (7.26) requires the bandwidth of the squeezed vacuum to be broad enough to justify the Markov approximation, and the bandwidth of the squeezed vacuum has been assumed sufficiently large ($\kappa/\gamma > 10$), while the results in Section 7.4 have been obtained for the squeezing bandwidth, which is comparable or even smaller than the atomic linewidth. It would be, of course, interesting to compare the two approaches in the same range of the squeezing bandwidths. It is possible to make such a comparison, and it has been done in [67]. Since the coupled-systems approach is valid for any value of κ, numerical solutions for the resonance fluorescence spectra obtained from the master equation (7.102) can serve as a reference for the spectra obtained by solving equations (7.65). It is particularly interesting to check how large κ must be to get a reasonable agreement between the two approaches. In Fig. 7.21 we have plotted examples of the spectra for (a) weak and (b) strong fields. Figure (a) shows an example of the spectrum for a special value of the Rabi frequency $\Omega/\gamma = 0.35$ for which the spectrum shows a dip at the center. As is seen for the squeezing

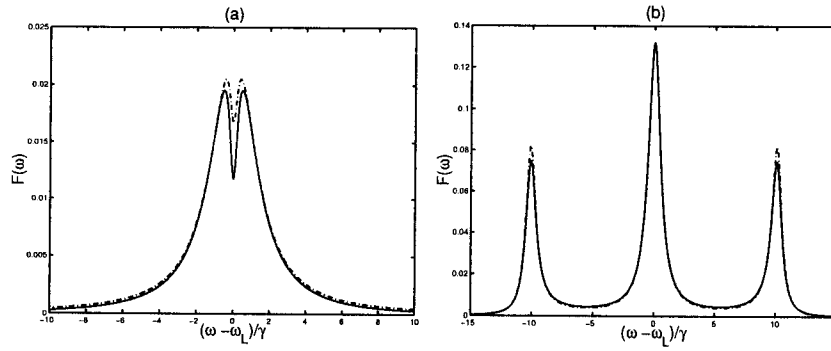

Fig. 7.21 Resonance fluorescence spectra plotted according to the coupled-systems approach (solid line) and the master equation (7.26) (dashed-dotted line). The parameters are: (a) $\kappa/\gamma = 40$, $\epsilon/\kappa = 1/8$, $\Omega/\gamma = 0.35$, and (b) $\kappa/\gamma = 10$, $\epsilon/\kappa = 0.125$, $\Omega/\gamma = 10$.

bandwidth $\kappa/\gamma = 40$, the master equation (7.26) reproduces the dip and it is in quite a good agreement with the spectrum obtained from the coupled-systems approach. Figure (b) shows an example of the spectrum for $\Omega/\gamma = 10$, and in this case $\kappa/\gamma = 10$, which means that the squeezing bandwidth covers one-third of the range of frequencies shown in the figure. This example shows convincingly that the bandwidth of squeezed light should be greater than the atomic linewidth but not necessarily greater than the Rabi frequency to justify the Markovian approximation. The sidebands are shifted slightly with respect to the coupled-systems result, but the central line fits almost perfectly for a squeezing bandwidth as small as $\kappa/\gamma = 10$. For the examples above, we have assumed that $\eta = 0.98$ in the master equation (7.102), and for better comparison the spectra are normalized to the same rate. Of course, as the values of the squeezing bandwidth κ/γ become larger and larger the Markovian approximation works better and the analytical results based on the master equation (7.26) are more reliable.

Acknowledgments

I would like to thank Professor Z. Ficek and Dr. A. Messikh for their cooperation on the subject.

REFERENCES

1. A. S. Parkins, in M. Evans and S. Kielich (Eds.), *Modern Nonlinear Optics,* Pt 2, Vol. LXXXV of *Advances in Chemical Physics*, Wiley, New York, 1993, p. 607.
2. B. J. Dalton, Z. Ficek, and S. Swain, *J. Mod. Opt.* **46**, 379 (1999).
3. C. W. Gardiner, *Phys. Rev. Lett* **70**, 2269 (1993).
4. H. J. Carmichael, *Phys. Rev. Lett.* **70**, 2273 (1993).
5. C. W. Gardiner, *Phys. Rev. Lett.* **56**, 1917 (1986).
6. H. J. Carmichael, A. S. Lane, and D. F. Walls, *J. Mod. Opt.* **34**, 821 (1987).
7. B. R. Mollow, *Phys. Rev.* **188**, 1969 (1969).
8. T. Quang, M. Kozierowski, and L. Lan, *Phys. Rev. A* **39**, 644 (1989).
9. A. Banerjee, *Phys. Rev. A* **52**, 2472 (1995).
10. J. M. Courty and S. Reynaud, *Europhys. Lett.* **10**, 237 (1989).
11. S. Smart and S. Swain, *Phys. Rev. A* **45**, 6863 (1992).
12. S. Smart and S. Swain, *Quantum Opt.* **5**, 75 (1993).
13. S. Smart and S. Swain, *Phys. Rev. A* **48**, R50 (1993).
14. B. R. Mollow, *Phys. Rev. A* **5**, 2217 (1972).
15. D. Grandclement, G. Grynberg, and M. Pinard, *Phys. Rev. Lett.* **59**, 40 (1987).
16. C. Szymanowski, C. H. Keitel, B. J. Dalton, and P. L. Knight, *J. Mod. Opt.* **42**, 985 (1995).
17. Special issue on atomic coherence and interference, *Quantum Optics* **6**(4) (1994).
18. C. Cohen-Tannoudji and S. Reynaud, *J. Phys. B* **10**, 345 (1977).
19. J. I. Cirac, R. Blatt, P. Zoller, and W. D. Phillips, *Phys. Rev. A* **46**, 2668 (1992).
20. J. I. Cirac and P. Zoller, *Phys. Rev. A* **47**, 2191 (1993).
21. Y. Shevy, *Phys. Rev. Lett.* **64**, 2905 (1990).
22. Z. Ficek, S. Smyth, and S. Swain, *Opt. Commun.* **110**, 555 (1994).

23. R. E. Slusher, L. W. Hollberg, B. Yurke, J. C. Mertz, and J. F. Valley, *Phys Rev. Lett.* **55**, 2409 (1985).

24. R. M. Shelby, M. D. Levenson, S. H. Perlmutter, R. G. DeVoe, and D. F. Walls, *Phys. Rev. Lett.* **57**, 691 (1986).

25. L. A. Wu, H. J. Kimble, J. L. Hall, and H. Wu, *Phys. Rev. Lett.* **57**, 2520 (1986).

26. N. P. Georgiades, E. S. Polzik, K. Edamatsu, H. J. Kimble, and A. S. Parkins, *Phys. Rev. Lett.* **75**, 3426 (1995).

27. C. W. Gardiner, A. S. Parkins, and M. J. Collett, *J. Opt. Soc. Am. B* **4**, 1683 (1987).

28. M. J. Collett, R. Loudon, and C. W. Gardiner, *J. Mod. Opt.* **34**, 881 (1987).

29. A. S. Parkins and C. W. Gardiner, *Phys. Rev. A* **37**, 3867 (1988).

30. H. Ritsch and P. Zoller, *Phys. Rev. Lett.* **61**, 1097 (1988).

31. A. S. Parkins, *Phys. Rev. A* **42**, 4352 (1990).

32. A. S. Parkins, *Phys. Rev. A* **42**, 6873 (1990).

33. G. Yeoman and S. M. Barnett, *J. Mod. Opt.* **43**, 2037 (1996).

34. J. I. Cirac, *Phys. Rev. A* **46**, 4354 (1992).

35. Z. Ficek, B. J. Dalton, and M. R. B. Wahiddin, *J. Mod. Opt.* **44**, 1005 (1997).

36. M. Bosticky, Z. Ficek, and B. J. Dalton, *Phys. Rev. A* **53**, 4439 (1996).

37. R. Tanaś, Z. Ficek, A. Messikh, and T. El-Shahat, *J. Mod. Opt.* **45**, 1859 (1998).

38. C. W. Gardiner and A. S. Parkins, *Phys. Rev. A* **50**, 1792 (1994).

39. W. S. Smyth, S. Swain, Z. Ficek, and M. Scott, *Phys. Rev. A* **57**, 585 (1998).

40. W. S. Smyth and S. Swain, *Phys. Rev. A* **59**, R2579 (1999).

41. A. Messikh, R. Tanaś, and Z. Ficek, *Phys. Rev. A* **61**, 033811 (1999).

42. P. L. Knight and R. Loudon, *J. Mod. Opt.* **34**, 709 (1987).

43. Q. Q. Turchette, N. P. Georgiades, C. J. Hood, and H. J. Kimble, *Phys. Rev. A* **58**, 4056 (1998).

44. M. J. Collett and C. W. Gardiner, *Phys. Rev. A* **30**, 1386 (1984).

45. H. Carmichael and D. F. Walls, *J. Phys. A: Math. Gen.* **6**, 1552 (1973).

46. J. Cresser, *J. Mod. Opt.* **39**, 2187 (1992).

47. W. H. Louisell, *Quantum Statistical Properties of Radiation*, Wiley, New York, 1973.

48. G. Yeoman, *Phys. Rev. A* **55**, 710 (1997).

49. H. J. Kimble and L. Mandel, *Phys.Rev. A* **13**, 2123 (1976).

50. W. S. Smyth and S. Swain, *Opt. Commun.* **112**, 91 (1994).

51. C. Cohen-Tannoudji, J. Dupont-Roc, and G. Grynberg, *Atom–Photon Interaction*, Wiley, New York, 1992.

52. C. Cabrillo, W. S. Smyth, S. Swain, and P. Zhou, *Opt. Commun.* **114**, 344 (1995).

53. M. Lax, *Phys. Rev.* **172**, 350 (1968).

54. S. Swain and P. Zhou, *Opt. Commun.* **123**, 310 (1996).

55. M. J. Collett, D. F. Walls, and P. Zoller, *Opt. Commun.* **52**, 145 (1984).

56. R. Tanaś, *Opt. Spectrosc.* **87**, 743 (1999).

57. S. Swain, *Phys. Rev. Lett.* **73**, 1493 (1994).

58. D. F. Walls and P. Zoller, *Phys. Rev. Lett.* **47**, 709 (1981).

59. R. Tanaś and T. El-Shahat, *Acta Phys. Slovaca* **48**, 301 (1998).

60. C. W. Gardiner, *Quantum Noise*, Springer-Verlag, Berlin, 1991.

61. E. S. Polzik, J. L. Sørensen, and J. Hald, *Appl. Phys. B: Lasers Opt.* **66**, 759 (1998).

62. A. S. Parkins and C. W. Gardiner, *Phys. Rev. A* **40**, 3796 (1989).

63. S. Tan, *J. Opt. B: Quantum Semiclass. Opt.* **1**, 424 (1999).

64. P. Kochan and H. J. Carmichael, *Phys. Rev. A* **50**, 1700 (1994).

65. P. R. Rice and H. J. Carmichael, *J. Opt. Soc. Am. B* **5**, 1661 (1988).

66. Z. Y. Ou, C. K. Hong, and L. Mandel, *J. Opt. Soc. Am. B* **4**, 1574 (1987).

67. R. Tanaś, *Acta Phys. Slovaca* **49**, 595 (1999).